MODIFICATION OF MATERIALS FOR HIGH OXIDATION RESISITANCE

A Dissertation

Presented to

the Faculty of the Graduate School

at the University of Missouri-Columbia

In partial Fulfillment

Of the Requirements for the Degree

Doctor of Philosophy

By

YEFER MAURICIO SUAREZ BUITRAGO

Dr. Mark A. Prelas

Dissertation Supervisors

Dr. Tushar K. Ghosh

JULY 2012

The undersigned, appointed by the dean of the Graduated Scholl, have examined the dissertation entitle

MODIFICATION OF MATERIALS FOR HIGH OXIDATION RESISITANCE

Presented by

YEFER MAURICIO SUAREZ BUITRAGO,

a candidate for the degree of doctor of philosophy and hereby certify that, in their opinion, it is worthy of acceptance.

_____

Dr. Mark A. Prelas, Nuclear Science and Engineering Institute

_____

Dr. Tushar K. Ghosh, Nuclear Science and Engineering Institute

_____

Dr. Sudarshan K. Loyalka, Nuclear Science and Engineering Institute

_____

Dr. Frank Feng, Department of Mechanical Engineering

_____

Dr. Alejandro Suárez-Alvites, Department of Chemical Engineering

“What we know is a drop of water, what we ignore is the ocean” (Isaac Newton).

To my beloved wife Dominike, my princess Anna, my unconditional supporter in all moment my Mom, my friend beyond this world, my Dad, and to my brothers and sisters.

ACKNOWLEDGMENTS

I want to express my deepest thanks and appreciation to my advisors, Dr. Mark Prelas and Dr. Tushar Ghosh for their advising, patience, encouragement, and unconditional support throughout this project. I would like to thank my dissertation committee for their suggestions about improving this work. I want to extend my appreciation to Dr. Adrian Mendez and Dr. Mike Peck for all their help since the beginnings of this project.

I would like to extent my gratitude to those who took their time to analyze my samples: Mr. Lou Ross, Jr. (Electron microscope), and Matthew Simones (Atomic force microscope). I would also extent my gratitude and thank to Dominike Merle-Johnson for her advice in the redaction of this dissertation.

I would like to extent my gratitude to the Nuclear Engineering Institute for this unique opportunity to pursue my degree.

TABLE OF CONTENTS

ACNOLEDGMENTS……...…ii

LIST OF FIGURES……v

LIST OF TABLES……..ix

ABSTRACT……x

CHAPTERS

1. INTRODUCTION……1
2. DESCRIPTION OF CORROSIVE ENVIRONMENTS……...6
    2.1. Production of hydrogen from sulfuric acid cycles
        2.1.1. Sulfur bromine hybrid cycle
        2.1.2. Sulfur iodine cycle
        2.1.3. Hybrid sulfuric cycle
    2.2. Catalysis process
    2.3. Effects of annealing and gas treatment of morphology of platinum
    2.4. Previously tested materials
3. EXPERIMENTAL SETUP AND CHARACTERIZATION METHODS…….20
    3.1. Annealing system “cold wall reactor”
    3.2. Diffusion reactor (FEDOA GEN V)
    3.3. Modifications of the sulfuric acid oxidation reactor (SAOR)
    3.4. CHARACTERIZATION METHODS
4. METHODOLOGY AND EXPERIMENTAL RESULTS……31
    4.1. Methodology
    4.2. Diamond treatment with platinum

4.2.1. Annealing in hydrogen atmosphere

4.2.2. Discussion

4.3. Stainless steel treatment with platinum

4.3.1. Annealing in hydrogen atmosphere

4.3.2. Discussion

4.4. Stainless steel treated with iridium

4.4.1. Discussion

5. CONCLUSION…….67

6. SUGGESTIONS FOR FUTURE WORK ……70

APPENDIX

I. ENERGY CONSUMPTION……..71

II. PROPERTIES OF MATERIALS……...74

REFERENCES...……..77

VITA……..……83

LIST OF FIGURES

Figure

2.1. Sulfur family of thermochemical cycles

2.2. Sulfur iodine cycle

2.3. Schematic representation of S-I cycle

2.4. Schematic of hybrid sulfur thermochemical process

2.5. Three- dimensional STM image of Pt cluster formed on HOPG without annealed.

2.6. SO_2 production rates over platinum group/titanium.

2.7. Decomposition of H_2SO_4 using $Fe_{1.8}Cr_{0.2}O_3$

3.1. Cold wall reactor systems

3.2. Internal view of cold wall reactor

3.3. Diffusion reactor (FEDOA GEN V)

3.4. Decomposition products from one mole of sulfuric acid as function of temperature

3.5. Design of decomposer simulator

3.6. Reaction chamber and quartz liners

3.7. Modified simulator flow path

3.8. Five liter collection and liquid trap

3.9. Sample holder

3.10. Oxidation reactor

4.1. Diamond samples untreated

4.2. Annealed process

4.3. Raman spectrum of untreated, sputter and annealing diamond samples

4.4. Raman spectrum of diamond sample 3 after 4 in OXR

4.5. Raman spectrum of diamond sample 3 after 8 in OXR

4.6. Micrograph of diamond samples in each process, selected for the Raman spectrum: (a) Sample untreated, (b) sample treated, (c) sample with annealing, (d) sample after the OXR (4 hours).

4.7. UV-Vis for the untreated (1), the sputtering (2), and (3) the annealing diamond samples

4.8 Sample 1 (untreated diamond)

4.9 Sample 2 (diamond with sputtering)

4.10 Sample 3 (sputtering and annealing)

4.11. .SEM micrographs of the: untreated (a), with sputtering (b), after annealing (c), after oxidation (d) diamond samples

4.12. EDS analysis of the untreated diamond sample

4.13. EDS analysis of treated diamond sample (after sputtering)

4.14. EDS analysis of diamond sample after annealing

4.15. EDS analysis of diamond sample after oxidation process

4.16. AFM analysis on untreated and treated diamond samples: (a) untreated, (b) after SP, (c) annealing and (d) after OXR

4.17. Raman spectrum of the untreated stainless steel sample

4.18. Raman spectrum for the stainless steel sample treated with platinum

4.19. Raman spectrum for the stainless steel sample treated after annealing process

4.20. Raman spectrum for stainless steel sample treated after 4 hours in the OXR

4.21. Micrograph of the stainless steel samples in each process, selected for the Raman spectroscopy. (a) Sample untreated, (b) sample treated, (c) sample with annealing, and (d) sample after the OXR (4 hours)

4.22. UV-VIS for stainless steel sample treated after sputtering process

4.23. UV-VIS for the stainless steel sample treated after annealing

4.24. Stainless steel untreated

4.25. Stainless steel treated with platinum

4.26. Stainless steel treated after annealing process

4.27. SEM images of: untreated (a), with sputtering (b), after annealing (c), after oxidation, and (d) stainless steel samples

4.28. EDS analysis of stainless steel sample in different points after sputtering process

4.29. EDS analysis of stainless steel after annealing

4.30. EDS analysis of stainless steel after oxidation process

4.31. SEM images of stainless steel samples treated with platinum, without annealing after 12 hours in OXR

4.32. EDS analysis of stainless steel samples treated with platinum, without annealing after 12 hours in OXR

4.33. AFM analysis on untreated and treated stainless steel samples: (a) untreated, (b) after SP, (c) annealing, and (d) after OXR

4.34. Raman spectrum of stainless steel treated with iridium

4.35. Raman spectrum of stainless steel treated with iridium after annealing

4.36. Raman spectrum for the stainless steel sample treated with iridium after 4 hours in the OXR

4.37. Micrographs of the stainless steel samples treated with iridium in each process, selected for the Raman spectroscopy. (A) Sample treated, (B) sample with annealing, and (C) sample after the OXR (8 hours).
4.38. Stainless steel treated with iridium
4.39. Stainless steel treated with iridium after the annealing process
4.40. SEM images of the stainless steel treated with iridium; (A) after annealing and (B) after oxidation
4.41. EDS analysis of stainless steel treated with iridium after annealing
4.42 EDS analysis of stainless steel with iridium after the oxidation process
4.43. AFM analysis on untreated and treated stainless steel samples treated with iridium: (a) annealing and (b) after OXR
4.44. AFM analysis of the iridium cluster during the annealing process: (a) nitrogen, (b) helium, (c) hydrogen, (d) argon

LIST OF TABLES

Table

1.1. Comparison between electrolysis, steam reforming and sulfur-iodine

2.1. Summary of the effects of the gas treatment and annealing time on of the particle size and shapes of the Pt/HOPG samples

2.2. Alloy screening list

3.1. Techniques used to characterize diamond, stainless steel and quartz

4.1. Diamond samples treated with platinum

4.2 Stainless steel treated with platinum

4.3 Stainless steel treated with iridium

4.4 Diamond treated with iridium

MODIFICATION OF MATERIALS FOR HIGH OXIDATION RESISITANCE

Yefer M Suarez Buitrago

Dr. Mark A. Prelas and Dr. Tushar K Ghosh, Supervisors

ABSTRACT

As a result of high oil prices and the increase effects of greenhouse gases due to the combustion of fossil fuels is necessary to find other sources of energy. Hydrogen has the potential to replace part of the fossil fuel used today and reduce the greenhouse effect. The sulfur iodine cycle and bromine cycle coupled with high temperature heat from the next generation of nuclear reactors IV (GEN IV) is a potential solution to reduce of the emission of greenhouse gases in the production of hydrogen as well as its economic advantages in large-scale electricity. This cycle starts with the decomposition of sulfuric acid to sulfur dioxide at high temperatures (825-920^{o}C), depending of the catalysis used. Prior to implementing this technology it is necessary to develop new materials to withstand the highly corrosive environmental conditions in the decomposition of an acid at high temperature. The diamond research group began an investigation to improve some materials to be used in the production of hydrogen from the decomposition of acids at high temperatures.

In this work, samples of polycrystalline synthetic diamond films were prepared with a thin film of Pt deposited on the surface by magnetron sputtering. Different thicknesses, which range from 0.1nm to 3nm, were deposited over the surface of the samples. The

coated samples were annealed in a cold wall and the diffusion reactors in an inert environment a temperature between 500^0C and 850^0C for 8 hours. The annealing process created a more stable mechanical bond and a carbon-metal interface with the diamond. The samples were characterized before and after each process using micro–Raman spectroscopy, UV-Vis (DRUV-VIS), energy dispersive spectroscopy (EDS) I-V and QDLTS. Surface morphology and elemental distribution were studied by back scatter scanning electron images or scanning electron microscopy (SEM) and atomic force microscope (AFM).

Preliminary results demonstrated that the samples exhibited the diamond Raman main vibration peak (1331 cm^{-1}) associated with Sp^3 bonds. I-V measurements taken at room temperature on the surface of the sample, with variable currents from nano-ampere (nA) to milliampere (mA) and voltage between ±10 volts, revealed a linear response and a positive slope. Based on the preliminary results of this study it is assumed that the process created a homogenous coating on the samples. The samples were exposed in a sulfuric acid decomposer system (SADS) developed at the University of Missouri-Columbia to test the corrosion rate of the treated samples. The samples were tested in 4, 8, 12, and 16 hours of exposure at temperatures between 825^0C -850^0C.

After SADS, the samples did not loose mass meaning that the diamond improved its resistance to withstand the conditions found in the production of hydrogen at high temperatures, as a result of the homogeneous platinum coating.

Stainless steel and quartz films were prepared with a thin film of Pt deposited on the surface by magnetron sputtering. The results showed that the stainless steel samples did

not lose mass after the same exposure time used in the diamond studies with the sulfuric acid decomposition system (SADS).

This study also tested iridium (Ir) deposition on diamond, stainless steel and quartz films. The results showed that the samples lose between 5-50% of their mass, depending on environmental conditions in the annealing process. In this research, hydrogen, argon, helium and nitrogen were used in the annealing process at different temperatures. Furthermore, the results indicated that the annealing process in the presence of hydrogen improved the coating process, and also increased the oxidation resistance of diamond and stainless steel coated with platinum and iridium, when exposed to the SADS environment.

CHAPTER 1

Introduction

Hydrogen is important as a transportation fuel. In the last decade, the Bush administration announced the "Hydrogen fuel initiate"[1] with the objectives of reducing the greenhouses gas emission into the atmosphere and also to design a plan to transition from the current carbon economy to a hydrogen economy[2,3].

To consider the hydrogen economy it is necessary to increase the production of hydrogen, but currently, hydrogen production is too low for the projected consumption demand. The world production of hydrogen is estimated at around 45 millions tons or 500 million cubic meters, per year[4], and the USA produces about 40% of the total. Hydrogen is primarily produced from methane.

Hydrogen is the most abundant element in the universe and the third most abundant in the earth[5]. Hydrogen gas does not exist on the earth or in the atmosphere in large quantities, it react quickly with other elements to form stables compounds[5]. The two most common compounds are water and fossil fuels (hydrocarbons).

There are several procedures for producing hydrogen; all processes involve splitting compounds that contain hydrogen and then capturing the hydrogen gas at the end. The hydrogen may also be used as an energy carrier. The best known process for producing hydrogen are electrolysis, steam reforming, sulfur bromine hybrid cycle,

hybrid sulfuric cycle and sulfur iodine (S-I). The first two are used today. Ninety percent of hydrogen manufactured today is created by steam reforming of methane[5,6]. The S-I process and sulfur bromine hybrid cycle are under development for the industrial production of hydrogen using nuclear energy. The above processes have their advantages and disadvantages from economic to its effects on the environmental (Table 1.1)[5].

The other process that is going to be used in the production of hydrogen is hybrid sulfur thermochemical cycle using nuclear energy. The U.S. Department of energy (DOE) is leading an initiative to develop and research the technologies needed to support hydrogen production as a carrier of energy[6]. This initiative includes the investigation of the advantages nuclear reactor as a potential energy for hydrogen production and the development of new materials capable of withstanding the harsh environments created a high temperature (850-1000 ^{o} C) in the decomposition of sulfuric acid for production of sulfur dioxide feed stock [7]. Some materials may be used depending on their characteristics in terms of their stability at high temperatures, when they are modified or treated with metals. This study examines diamond and stainless steal which are good candidates when they are treated with metals, including platinum and iridium.

Corrosion resistant carbons, such as diamond, are promising materials in several fields, like electron emission devices, fuel cells and hydrogen storage. Diamond properties, (i.e. highest thermal conductivity, resistance to corrosion, and toughness to radiation), make it an excellent material when it is modified by the incorporation of impurities such as metals. Metal-Diamond base materials (Me:Db) can be used as a

support material for catalysis (i.e. catalytic electrodes), and can enhance the oxidation resistance properties of diamond when it is combined at elevated temperatures[8]. Diamond offers several advantages over carbon (sp^2 – bonded) electrodes, such as activated carbon, carbon black, and graphitized carbon. Sp^3 – bonded carbon, namely diamond, is corrosion resistant and offers structural stability. In contrast Sp^2 – bonded carbon is susceptible to corrosion and micro structural degradation during anodic polarization[9]. Studies also show that modified diamond supported catalysts exhibited higher catalytic activity when compare to activated carbon-supported catalysts[10].

The first objective of this research was to investigate materials that can tolerate the conditions present in the sulfuric decomposition cycle. The first task of this objective was to test materials that have high resistance to corrosion at high temperatures when are exposed in the sulfuric acid cycle decomposition. Natural diamond, stainless steel, quartz, platinum, and iridium were selected due to their high melting point and high resistance to corrosion. In previous work, the boron treated diamond, titanium treated synthetic diamonds, silicone carbide, quartz, platinum, and stainless steel were tested in the development, design and construction of the sulfuric acid decomposition system by the Diamond Research Group of the Nuclear Science and Engineering Institute at the University of Missouri (MU-DRG)[3]. As a result of MU-DRG research, was necessary to continue the research with those materials in special diamond, stainless steal, quartz and platinum.

The second objective of this research was to investigate the performance of different materials vs. modified materials under a simulated acid decomposition. As a result of this investigation (1) diamond treated with platinum improved corrosion resistance in harsh environments, such as the sulfuric acid decomposition system or oxidation reactor (OXR)[11]. (2) Stainless steel 404 and 304 were treated with platinum and showed improved resistance to corrosion in harsh environments, like the case of the decomposition of sulfuric acid decomposition. Those materials also improved their resistance to corrosion when the annealing process was in a hydrogen atmosphere[11].

The third objective of this research was to develop a procedure to increase the oxidation resistance properties of materials, for use in the sulfuric acid decomposition cycle.

Table 1.1[4]: Comparison between electrolysis, steam reforming and sulfur-iodine

	Electrolysis	**Steam Reforming**	**Sulfur-Iodine**
Advantages	- Simplest method requiring only a supply of water and electricity. - Environmentally friendly - Proven technology - Ideal for remote locations - Independent of fossil fuels - Potential for electrical peak-shaving	- The most efficient method of producing hydrogen today. - Proven technology - Near term nuclear capability - Lowest production cost - Contributes to nuclear S-I development	- High efficiency - Low production cost - Environmentally friendly - Independent of fossil fuels
Drawbacks	- Requires electricity. Electricity production is comparatively inefficient, expensive, and potentially polluting. - Highest production cost	- Dependent of fossil fuels - Produces CO2. - Must be in close proximity to the nuclear reactor	- In early phase of development - Must be in close proximity to the nuclear reactor
Assumptions	Capital cost of an electrolysis plant is $30.97 per GJ of yearly hydrogen production or $977 per kW-hydrogen of plant capacity.	Capital cost of an electrolysis plant is $11.443 per GJ of yearly hydrogen production or $361 per kW-hydrogen of plant capacity.	Capital cost of S-I cycle plant is $315 per kW-thermal or $630/kWhydrogen of plant capacity
Efficiency	25-45%	70%	50%
Preliminary Production Cost Estimate	$2.70/kg to $4.87/kg hydrogen	$0.92/kg hydrogen	$1.22/kg hydrogen
Schedule to Implementation	Currently available. Improvements possible with more development	Test production with nuclear facility scheduled for operation in 2008	Test production with nuclear reactor in greater than 10 years

CHAPTER 2

Description of Corrosive Environments

The development of the hydrogen economy program, included research of advanced nuclear reactors as energy sources for hydrogen production. The Department of Energy (DOE) "Nuclear Hydrogen Initiative" has identified three reactors from generation IV[12] that have the potential to provide the thermal energy needed for large scale hydrogen production from the sulfuric acid cycles. These reactors are gas-cooled reactor, molten salt reactors and very high temperature gas reactor.

2.1. Production of hydrogen from sulfuric acid cycles.

2.1.1. Sulfur bromine hybrid cycle

This cycle is a variation of the pure thermochemical cycle, which is called the hybrid cycle (Figure 2.1)[13]. The sulfur bromine cycle has been developed by CEC joint center at Ispra since 1974, and is called Euratom Mark. The present cycle consists of the three reactions[12]:

$2HBr \rightarrow H_2 + Br_2$ (electrolysis) (1)

$SO_2 + Br_2 + 2HO_2 \rightarrow 2HBr + H_2SO_4$ (90^oC) (2)

$H_2SO_4 \rightarrow H_2O + SO_2 + ½\ O_2$ (850^oC) (3)

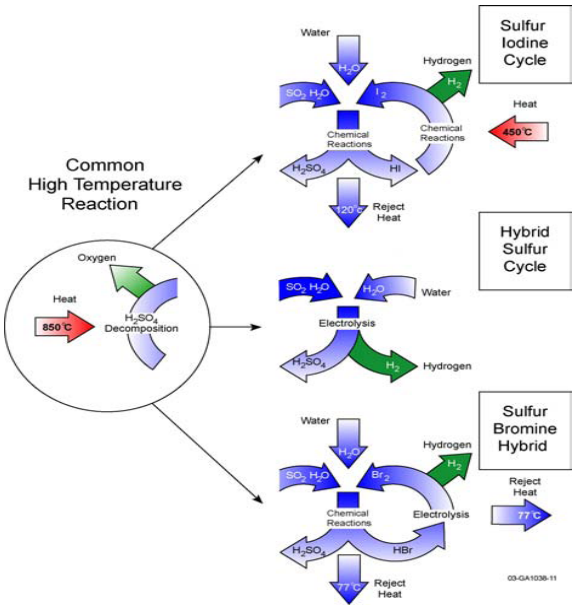

Figure 2.1[13]Sulfur family of thermochemical cycles

The electrolysis process is necessary to obtain hydrogen and bromine. The characteristic in the electrolytic process include a voltage of 200mA/cm and 350 ^{o} C which is 0.85v(less that the water electrolysis). Platinum is used as a homogeneous electrocatalyst. These metals reduce the overvoltage at the cathode [12].

2.1.2 Sulfur iodine cycle.

The sulfur iodine (S-I) cycle is a series of thermochemical process use to produce hydrogen. This cycle consists of three reactions (Figure 2.2)[13] whose net reactant is water and whose products are oxygen and hydrogen. The three reactions are:

$$2H_2SO_4 \rightarrow 2SO_2 + 2H_2O + O_2 \ (850\,^{o}\,C) \qquad (1)$$

$$I_2 + SO_2 + 2H_2O \rightarrow 2HI + H_2SO_4 \ (120\,^{o}\,C) \qquad (2)$$

$$2HI \rightarrow I_2 + H_2 \ (450\,^{o}\,C) \qquad (3)$$

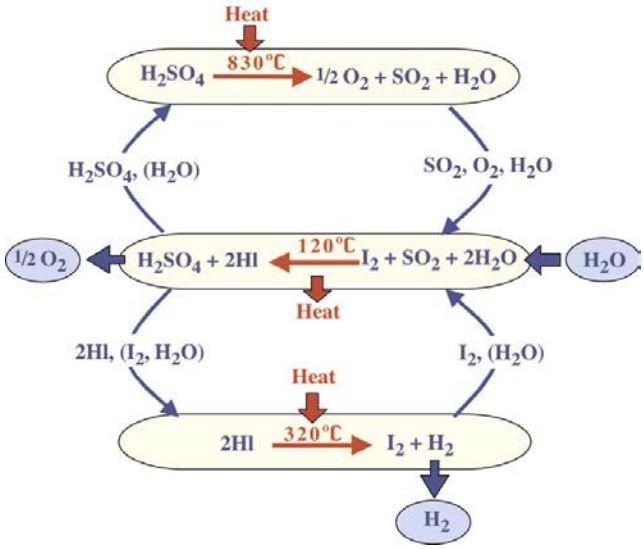

Figure 2.2[13] Sulfur iodine cycle

In the first reaction (eq. 1), the sulfuric acid is vaporized and superheated to 850^0C, and a result the acid is discomposed into water, oxygen and sulfur dioxide. After this reaction, the sulfuric dioxide is combined with water and iodine in the Bunsen reaction (eq 2), which produces hydrogen iodine and sulfuric acid. In the last reaction, hydrogen is discomposed in iodine and hydrogen gas is liberated. The iodine and sulfuric acid are recycled and back to the Bunsen reactor and sulfuric acid decomposer (Figure 2.3)[14].

The S-I cycle involves operations with corrosive chemical at temperatures between 800 and 1000 °C. The selection of materials with sufficient corrosion resistance under these conditions is of a key aspect for the economic viability of this process. The materials suggested include the following classes: refractory metals, reactive metals, super alloys, ceramics, polymers, and coatings[14]. Some materials suggested include

tantalum alloys, niobium alloys, noble metals, high-silicon steels, several nickel-base silicon carbide SiC, grass, silicon nitride Si_3N_4[14].

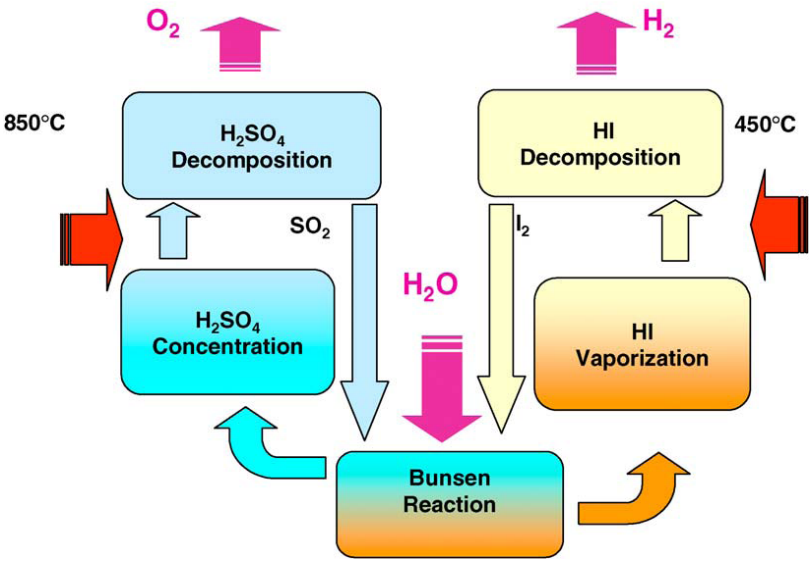

Figure 2.3[14] Schematic representation of S-I cycle

The S-I cycle has been proposed as a way to supply hydrogen for a hydrogen-based economy. With an efficiency of around 50%, it is more efficient than electrolysis[15]. It does not require hydrocarbons like current methods of steam reforming but requires heat from combustion, nuclear reactions, or solar heat concentrators.

2.1.3 Hybrid sulfuric cycle.

The hybrid sulfuric cycle (often called Westinghouse cycle) combine electrolysis and thermochemical process for decomposing water into hydrogen and oxygen (Figure 2.4)[16].

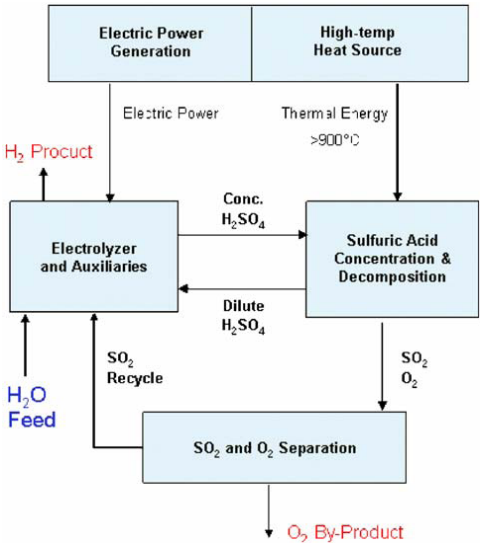

Figure 2.4[16] Schematic of hybrid sulfur thermochemical process

In the thermal decomposition, the sulfuric acid is decomposed into sulfur trioxide steam, the sulfur trioxide is decomposed into sulfur dioxide and oxygen at high temperature (eq. 1)[17].

During the electrolysis process, the sulfuric acid and hydrogen is obtained from water and sulfur dioxide mixture at low temperature (eq. 2)[17].

$H_2SO_4 \rightarrow H_2O + SO_3 \rightarrow SO_2\ (g) + H_2O\ (g) + ½\ 0_2(g)$ (thermal decomposition, 850°C) (1)

$2H_20 + SO_2\ (g) \rightarrow H_2SO_4 + H_2\ (g)$ (electrolysis, 110°C) (2)

The presence of sulfur dioxide along with water in the electrolyzer reduces the required electrode potential well below that required for the pure–water electrolysis. The theoretical values to decompose water is 1.23V or higher[17], depending of the electrolyzer.

In comparison with 0.17V required for electrolysis with sulfur dioxide, this is less than 15% of the voltage needed in commercial water electrolyzer[17].

In addition, using only sulfuric acid for the thermochemical processes minimizes the required chemical stock in the hydrogen plant well below what is required for the sulfur–iodine pure thermochemical cycle. Thus, the hybrid process has potential advantages with regards to both pure electrolysis and pure thermochemical procesess[17].

The main problems to be solved before the hybrid-sulfur cycles is developed for commercial use are improved materials that can withstand high temperatures and high concentrations of acids for long period of time.

In recent years an effort began to seek methods to improve and design new materials to withstand the conditions present in the production of hydrogen from the sulfuric acid cycles at high temperatures. Two of these materials are platinum and iridium. These materials were selected for high corrosion resistance and high efficiency as a catalyst.

2.2. Catalysis process

Catalytic activity of supported metals for sulfuric acid decomposition reaction is the key in the thermo-chemical cycles process to produce hydrogen through a series of chemical reactions, where the net results is the productions of hydrogen and oxygen from the water at lower temperature that direct thermal decomposition.

The catalytic-chemicals in this process are recycle, and the heat source for those reaction can be obtain from nuclear or solar power. Hydrogen is produced without greenhouse gases and also is independent from fossil fuels[12].

The sulfuric acid is the base of thermo chemical cycles. Those including sulfur-iodine cycle, the hybrid sulfur cycle, and the sulfur-bromine cycle. The decomposition reaction of sulfuric acid taken two processes; a non-catalytic thermal decomposition of the acid to form gaseous SO_2 and H_2O at temperature of 350 ^oC, followed by catalytic decomposition of SO_3 at average temperature 800-850 ^{o} C. The SO_2 is the half of the water splitting reaction and is a product from the cycle [18].

The catalytic decomposition of SO_3 requires improving materials that are going to be used in this process, and also to keep a high efficiency in the reaction of the decomposition of SO_3. The annealing process is very important to increase the efficiency of the materials that are going to be use as catalytic for high temperature use. The platinum is ones of the most important catalytic materials.

2.3. Effects of annealing and gas treatment of morphology of platinum.

The morphology of the metal clusters plays an important role in determining the catalytic activity of many reactions[19]. Thus, it is important to determine how the particle size and shape affect the catalyst activity. The metal cluster has been the point of interest of many studies in the last years, mainly with the use of scanning tunneling microscopy (SEM) and electron microscopy (TEM) [20].

The different gases used in the annealing process, have strong in influence on the transformation of shape of the Pt/ "highly oriented pyrolytic graphite" (HOPG) clusters as a function of annealing time[19] (Table 2.1).

Table 2.1[19] Summary of the effects of the gas treatment and annealing time on of the particle size and shapes of the Pt/HOPG samples

Gas treatment	Annealing time (h)	Particle size (Å)	Particle shape
Ar	0	~ 160	oval
	4	~ 150	spherical
	12	120–150	spherical
	24	length: ~ 200 width: ~ 75	polyhedral elongated
H_2	0	~ 160	oval
	4	20–70	spherical
	12	length: ~ 90 width: ~ 30	polyhedral elongated
N_2	0	~ 160	oval
	4	length:~ 100 width: ~ 50	polyhedral elongated
	12	~ 80	cubo-octahedron
	24	~ 70	spherical

The deposited Pt cluster on highly oriented pyrolytic graphite (HOPG) without annealing pretreated shows a large elongated cluster and aggregations of small particles. It appears is a bright spot (Figure 2.5)[19].

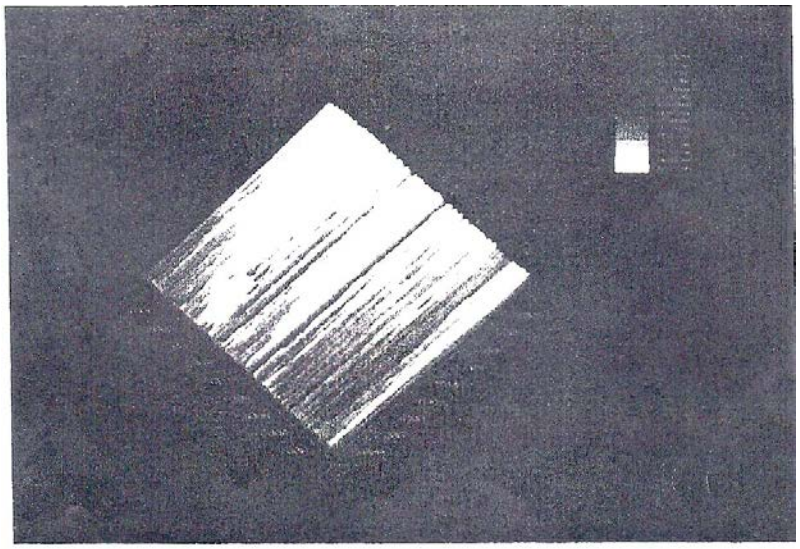

Figure 2.5[19] Three- dimensional STM image of Pt cluster formed on HOPG without annealing.

The Pt is annealed with Argon atmosphere for 4 hours at 600 ^{o} C. The cluster (Pt) change from longer aggregations of smaller clusters to more uniform and spherical shape, also their size decreased from 35Å to 150Å in average[6, 20]. When the sample is annealed for 12 hours at the same temperature, the shape of Pt cluster are still quite spherical, but some cluster now appear to have rounded corners[19]. This transformation is more obvious at 24 hours [19] and the clusters have become elongated. After 24 hours the clusters have obtained an equilibrium shape at 600 ^{o}C (Table 2.1). The reason why the clusters change their shape is because the impurities (hydrocarbons) are discomposing and adsorbing onto the surface during annealing [19, 21].

Pt is annealed in hydrogen atmosphere at 600 ^{o}C for 4-12 hours. After 4 hours, the form of Pt clusters is quite uniform and spherical. This observation is consistent with the observed in Ar annealed samples[19]. “The explanation for this is that the hydrogen reacts with carbons to produce hydrocarbon species and those effects the transformations of the

Pt clusters"[19]. The transformation from spherical to the elongated shape is more evident at shorter annealing time with H_2 that Ar. This observation indicates that the hydrocarbon impurities effect the transformation of the Pt cluster[19, 22].

The Pt is annealed in nitrogen atmosphere at 600 ^{o}C for 4, 12, and 24 hours. After 4 hours, the Pt cluster appears elongated polyhedral and no spherical particle or cluster appears during this period of time[19]. The cube-octahedron shape of the Pt cluster is observed in the sample annealed after 12 hours. The transformation of the Pt cluster is more obvious after 24 hours of annealing. The shape of the Pt cluster is spherical (Table 2. 1), meaning that the morphology of the cluster has obtained an equilibrium structure[23].

The catalysis morphology (size and shape) in the case of platinum is influenced by the temperature, annealing time and by the presence of gases [19, 22]. When the platinum was deposited in other substrates, the morphology of the cluster or particles change.

The thermal treatments have been found to improve surface morphology of metal film. The Pt/Cr thin film was deposited on $Si_3N_4/SiO_2/Si$ substrates by electron-beam evaporation. The evaporated Pt film was annealed at 600^{o}C to 1200 ^{o}C in N_2 atmosphere. After the annealing process, the size of Pt was improved and also its shape too. From 600^{o}C to 1200^{o}C the pinholes grown by surface diffusion and at final the Pt film is transformed in islands[22].

2.4 Previously tested materials

The decomposition of H_2SO_4 takes place in two steps, a non-catalytic thermal decomposition of the acid to form gaseous SO_3 and H_2O at 350 ^oC, followed by the catalytic decomposition of the SO_3 at 850^oC to produce SO_2 and O_2 products [24]. The reduction of SO_3 requires a catalyst that may work at extremely high temperatures and under exposure to chemically aggressive environments that can destroy most catalysts within a short time. Platinum group metals, platinum-supported barium sulfate, Cr substituted for Fe oxide catalysts, and some metallic alloys have or are being tested to catalytic decomposition of SO_3 at high temperatures[24].

"The platinum group metals (PGM), including Pd, Pt, Rh, Ir and Ru has been investigated on different substrates including titanium, Al_2O_3 between others, in the production of hydrogen from by splitting water in the thermochemical sulfur-based cycles"[24]. The sulfur dioxide production for PGM catalysis is higher to Pt and Pd (softer metals) than for Rh, Ir and Ru (harder metals). The Pt can withstand the conditions for sulfuric decomposition cycle (Figure 2.6)[24], but the SO_2 production rate over Pd and Pt catalysis declined rapidly as results of the sulfate formation[24] and some cases due a formation of voltaic acid salts as consequence of the environmental conditions[25].

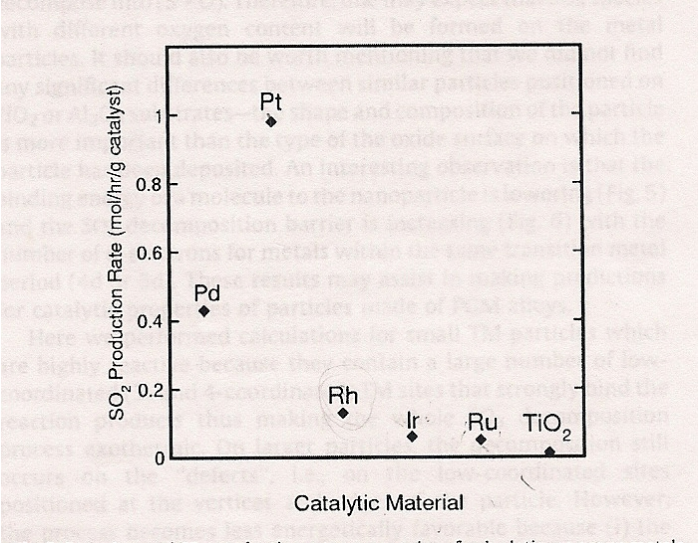

Figure 2.6[24] SO_2 production rates over platinum group/titanium

Various platinum-supported Barium sulfate catalyst have employed for SO_3 decomposition in sulfur-iodine cycle to produce hydrogen. Barium sulfate as a support has been prepared by different methods, i.e., using ethylene glycol(EG) and water, by dispersion method and EG and propanol by spray pyrolysis[26]. Under identical conditions, the 1.0Pt/$BaSO_4$ catalyst showed the highest catalytic performance because of high surface area and small particle size of platinum. This method showed the highest catalytic activity at 750 ^oC compared with others catalysts [26].

The activity and stability of Cr substituted Fe oxide catalysts were studied for the sulfuric–iodine acid decomposition reaction[27]. The catalytic activity of the samples in the decomposition of sulfuric acid was measured with gas chromatograph (SO_2 yield). Both substituted and unsubstantiated iron oxide samples (Figure 2.7) were found to be active for decomposition of sulfuric acid in the temperature range of 500-800^oC. The maximum activated was obtained at 800^oC. The activity of catalyst samples was found to be stable

up to 10 hours run. The formation of sulfates is present in the process. $Fe_{1.8}Cr_{0.2}O_3$ is promising active and mixed oxide catalyst for the SO_3 decomposition[27].

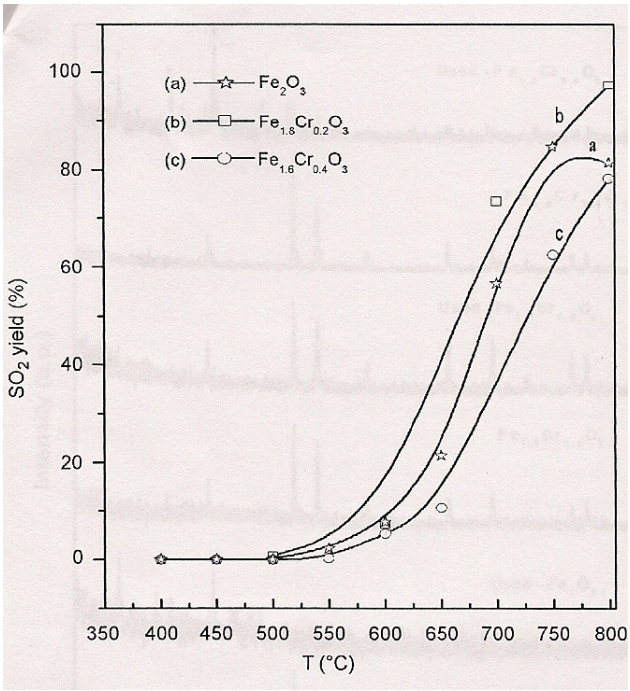

Figure 2.7[30] Decomposition of H_2SO_4 using $Fe_{1.}8Cr_{0.}2O_3$

Preliminary static corrosion, screening test has identified potential metallic alloys for use in the construction of the sulfuric acid decomposition loop (Table 2.2). The corrosion rates of three commercially available alloys, Saramet #23, Saramet #35 and zecor, are found to approach those accepted by the chemical industry (~0.1mm/year). Those alloys have a corrosion rate constant after some time[28].

Table 2.2[28] Alloy screening list

Alloy	Exposure time, hours	Corrosion rate, mm/yr
C-22, nickel-based alloy	96	10.0
I-800 nickel-based alloy	96	3.1
I-617 nickel-based alloy	72	8.0
Hastelloy D-205 nickel-based alloy	120	2.1
Hastelloy B3 nickel-based alloy	72	4.4
418, Stainless steel	96	5.8
430, Stainless Steel	96	1.8
440C, Stainless Steel	96	3.3
446, Stainless Steel	96	2.0
Zecor, iron-based	96	2.0
Saramet #23, iron-based	384	0.9
Saramet #35, iron-based	480	0.8

CHAPTER 3

Experimental setup and characterization

This chapter describes the experimental system employed in the annealing, sputtering and oxidation process, such as the cold wall reactor, diffusion reactor and oxidation reactors. The reactors used in this research were designed and build by the diamond research group of the Nuclear Science and Engineering Institute of the University of Missouri-Columbia.

3.1. ANNEALING SYSTEM "COLD WALL REACTOR".

The cold wall reactor (Figure 3.1) was designed by the diamond group research with the objective of improving the process of annealing for different materials at a small scale[29]. In this research, the reactor was used to modify the surface of diamond, stainless steel and quartz. Those materials were treated in the sputtering machine with a platinum and iridium targets prior to the annealing process.

Figure 3.1 Cold wall reactor systems

The internal setup of the reactor (Figure 3.2), is composed of two electrodes (A), this where the power source is connected to the system from an external power supply (B) and at this point the current is applied to the reactor. The purpose of the current is to heat up the sample and the reactor. The current pass through a filament wire (C). The wire is made of tungsten, with a diameter 0.55mm diameter. The tungsten can withstand high temperature. The wire is wrapped around the boron nitrite cylinder (D). Inside the cylinder there is a graphite cylinder (E). The graphite is able to withstand the high temperatures. At the top of the graphite cylinder is where the sample is inserted (F). A thermocouple (G) omega type K is used to monitor the temperature. The cylinders are on a graphite base (H).

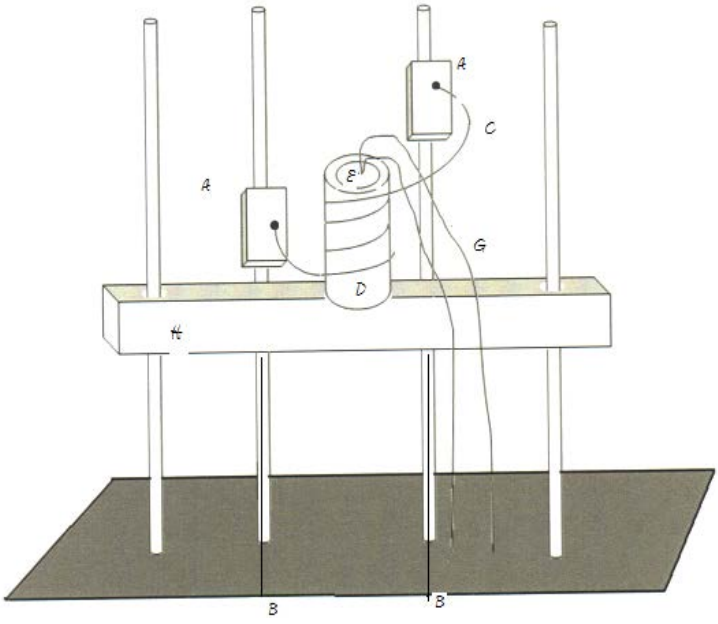

Figure 3.2 Internal view of cold wall reactor

Once the reactor is setup and the sample is in place, a pump vacuums out the air inside of the reactor. This creates a negative pressure within the reactor. The gas (helium,

argon and/or hydrogen) is introduced to purge the system and allows greater temperatures. After ten minutes, the flow of gas decreases to 20 mm Hg and the pump continues to generate a negative pressure. The power of the system is increased to five minutes to raise the temperature of the sample. While the experiment is running, cold water flows through the wall of the reactor. The water keeps the walls of the reactor cold while the reactor reaches the desired temperature. When the experiment is completed, the power is cut off and the flow of gas is stopped. The pump vacuum and the flow of water are keeping continuous until the temperature of the reactor reaches the environmental temperature[8, 29].

3.2. Diffusion reactor (FEDOA GEN V)

The FEDOA GEN V reactor is designed for the diffusion of impurities in wide band gaps films, and is a modification of MOD: FEDOA[35, 36] which was design by the diamond research group[29]. The objective of this design was to improve the process of annealing at higher temperatures, increased bias and lower pressure[29]. The FEDOA GEN V (Figure 3.3) consists of a base of stainless steal plate, a vacuum vessel and bias design, a substrate holder of boron nitride, gas flow meter, a pressure meter, thermocouples, amp and volt meter, a high voltage AC and DC power supply, and multiple photon source[36] (lasers). During operation the reactor is maintained at low pressure by a turbo vacuum pump, a drytel R 30 turbo molecular dry pump. Hydrogen is used in the reactor to assist in removing the oxygen molecules along with helium, argon and nitrogen. The gases help maintain an inert environmental during the samples treatment.

Figure 3.3 Diffusion reactors (FEDOA GEN V).

3.3. Modifications of the sulfuric acid oxidation reactor (SAOR):

The SAOR developed and tested by Michael Peck[3], which is described with more details in his dissertation[3]. In the next paragraphs are a summary of the more important features of this reactor. Also some modifications made to the reactor are described.

The design of the reactor starts with the construction of a sulfuric acid decomposer simulator to reproduce the temperature expected for the thermo chemical process as well as the pressure.

The minimum temperature needed to decompose one mole of sulfuric acid in sulfur dioxide and sulfur trioxide is 800^{o}C. This produces 0.60 mol percent of sulfur trioxide[36] (Figure 3.4)[3].

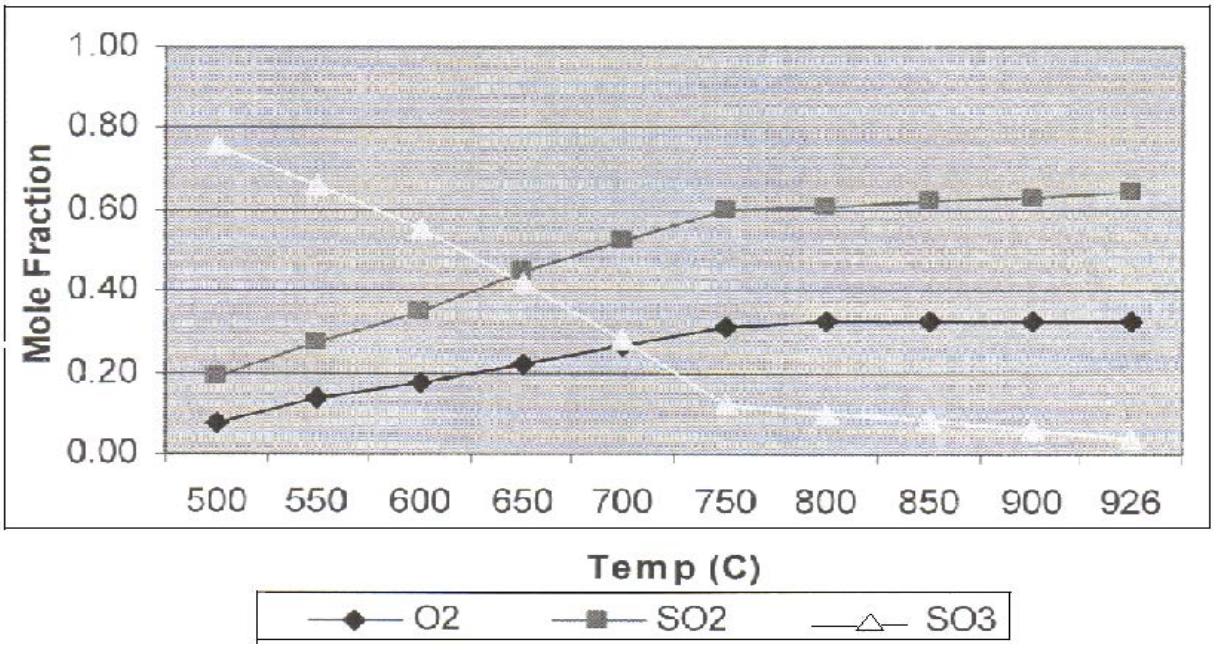

Figure3.4[3]. Decomposition products from one mole of sulfuric acid as function of temperature

The sulfur dioxide efficiency increased with decreasing process pressure based on a sulfuric acid decomposition kinetic model using the Aspen[3]. Based on the limitations of constructions for the high pressure laboratory apparatus, the simulator design pressure was limited to 1.10 bars[3].

The simulator design chosen was a closed cycle flow path with the objective that it mach the proposed sulfur iodine and hybrid sulfur cycles [13, 16]. The only feedstock added is water to the closed cycles, and the remaining reactants (sulfur dioxide, sulfur trioxide and oxygen non-condensable), are recycle. The simulator design consists of five

parts in a closed loop (Figure 3.5)[3]; sulfuric acid boiler, vapor super heater, reaction chamber and furnace, condenser and pressure (vent).

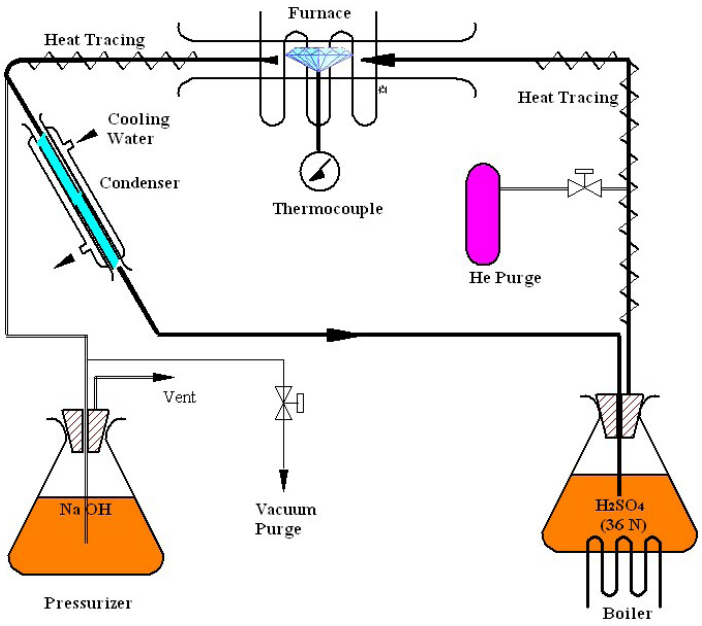

Figure 3.5[1,3] Design of decomposer simulator

The reaction chamber (modification), is made from incoly (AISI 446 stainless steel) of diameter 1 ½ that can accommodate a sample holder with a ½ inch radius[3]. A quartz lining was added to the simulator process piping to maintain decomposition product flow by reducing the building up of corrosion products[3]. The 1½ inch incoloy pipe was reinstalled into the reaction chamber. "The pipe was lined with a 45 mm by 35 mm GE Type 214 Quartz tube. The inside diameter of the tube was chosen to maximize sample holder space while allowing for radial thermal expansion stress as the quartz is heated to 926°C temperature. An end cap was constructed from 32 mm quartz tube with a 34 mm inside diameter. The rod and tube was cemented using Ceramacoat™ 503-VFG-C[1]. A ¾ inch diameter penetration was machined into the inlet of the reactor chamber

quartz tube"[3]. An 18 mm outside diameter quartz tube was cemented into the penetration. This 15 inch long tube was secured in the one-liter Pyrex™ acid boiler. The sealed flow path was encased in ¾ inch stainless steel tube adapted to the 1 ½ inch Incoloy pipe. The stainless steel tubing provided secondary confinement (Figure 3.6)[3].

Figure 3.6[3] Reaction chamber and quartz liners

In the same form, a ½ inch penetration was machined into the exhaust side of the 33 mm quartz tube. An 11 mm quartz tube was cemented into this penetration to transfer the discharge flow to the glass condenser. This arrangement provided a sealed flow path from the reaction chamber to the condenser[3]. This quartz tube was also encased in a ½ inch stainless steel tube adapted to the 1½ inch Incoloy pipe. A second removable quartz end cap was constructed on the exhaust end of the reaction chamber quartz tube[1].

The simulator process flow path was modified from closed to open cycle (Figure 3.7)[3], for the following reasons:

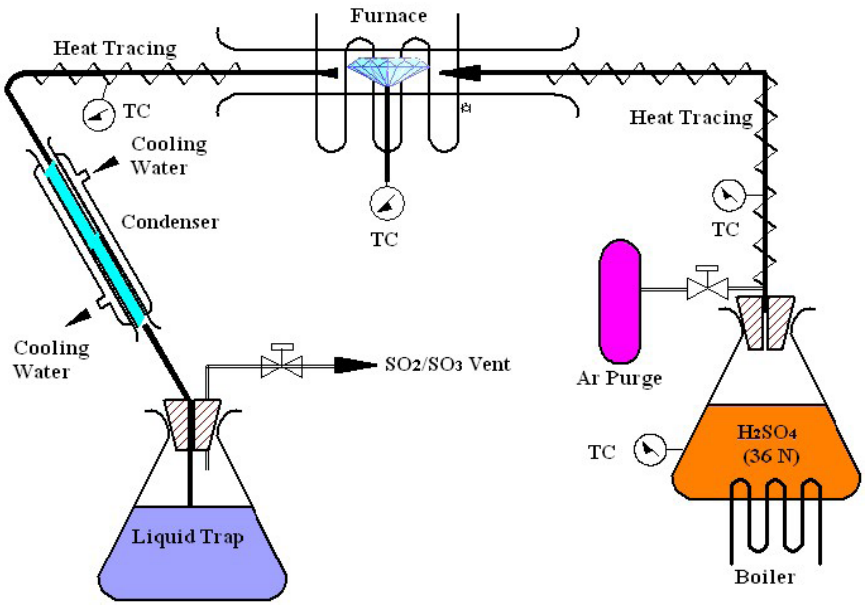

Figure 3.7[3] Modified simulator flow path

(1) avoid the accumulation of corrosion products in the boiler, (2) maintain the purity of the sulfuric acid in each operating cycle and, (3) verify the flow monitoring and the accumulation of reactants[6].

The addition of a five liters flask to collect the condensable fluids exiting the condenser (figure 3.8), with the purpose of containing all of the condensable reactants for a long period of operation (operating cycle).A gas exhaust was added at the top of this flask; then the gases passed through a second water cooled condenser (Figure 3.8) to trap any condenser material that may be carried. A second two liter liquid trap was added at the discharge of the second condenser; at the exhaust a second liter liquid trap was added

pump to eject the decomposition gases to the laboratory vacuum system from the top of the liquid trap[3].

Figure 3.8 Five liter collection and liquid trap.

The last modification was the addition of a 250 milliliter funnel at the top of the boiler to replenish the supply of sulfur acid to the boiler. A new sample holder (Figure 3.9) was made 14 mm outside diameter quartz tube. The sample holder could accommodate up to eight samples. These modifications eliminated the decomposition products or sulfuric acid contact with any metal components[3].

Figure 3.9.Sampler holder

The simulator has been in used from March 2008 (Figure 3.10), for four, six, eight, twelve, sixteen and twenty four hours at 870 ^{0}C without loss of flow or acid leaks and no plugging from corrosion products was observed. No mechanical damage was observed after the new quartz sample holder was removed following the last modification test.

Figure 3.10 Oxidation reactor

3.4 Characterization methods

A variety of characterization methods were used on diamond, stainless steel and quartz before and after each treatment. This is fundamental to understand the properties related with the modified surface by diffusion of impurities. Each characterization tool provides information complementary to other techniques (table 3.1). The samples were characterized by Raman spectroscopy, UV-Vis, I-V, SEM, EDS, and AFT.

Table 3.1.Techniques used to characterize diamond, stainless steel and quartz.

Technique	**Information**
Micro-Raman	Spectroscopy
UV-VIS	Spectroscopy
I-V	Electrical properties
SEM	Microscopy
EDS	Identification (elemental)
AFM	Spectroscopy

I-V- current voltage measurement

SEM- Scanning electron microscopy

EDS- Energy dispersive Spectroscopy

AFM- Atomic force microscopy

CHAPTER 4

Methodology and experimental results

Part of the information presented in this chapter has been presented at various conferences such as; 1) 2007 American Nuclear Society International Conferences Washington DC, 2) 2008 Gordon Research Conferences. High temperature materials, processes & diagnostic July 20-25, Colby College, Waterville, 3) 2008 ME International Conference of the Electrical Engineering Department of the Santo Tomás University in Tunja-Colombia, 4) 2010 Springfield annual meeting of the NASA-Missouri Space Grant consortium, and 5) 2011 Proceedings of the twentieth annual meeting of the NASA-Missouri Space Grant consortium in Saint Louis, MO.

One of the objectives of this research was to increase the oxidation resistance properties of materials such as diamond films (diamond type II/A plates) obtained from Harris international, New York. Platinum and iridium were used to increase the diamond resistance because of their high resistance to corrosion. Three samples with the same shape (1 cm^2 by 0.02cm thick) were selected (Figure 4.1). Prior to treatment, a cleaning procedure was performed. Before and after each process the samples were characterized with the objective to see the behavior of the samples after each process.

Raman analysis was used to determine any modifications to the diamond structure and stress in the diamond crystal (plate). Optical analysis using a Scanning Electron Microscopy (SEM) was performed to identify the morphology of the platinum on

diamond, element identification by energy dispersion x ray spectroscopy (EDS), volt-current characteristics (I-V) were used to study the diffusion of elements, UV-Vis spectroscopy, and Atomic force microscopy (AFM) was used to identify the surfaces change after each process.

Figure 4.1 Diamond samples untreated

4.1 Methodology

After the samples were clean, Pt was sputtered process on both sides of the sample, 50 minutes each side. The sputtering process was performed in a Denton vacuum, LLC, Desk IV sputter with an argon atmosphere. The thickness of the deposition was 1KÅ and the target was platinum.

After the sputtering, the samples went through an annealing process. A cold wall reactor at a low pressure (10x2Pa) was used, in a hydrogen atmosphere. The treatment temperature was 450-500^{o}C for 5 hours. A modified version of FEDOA[29] was used to improve the annealing process at higher temperature and vacuum. The temperature and

vacuum were 700^{o}C and 10x4 Pa, respectively for 3 hours in a hydrogen atmosphere. After the annealing process, the samples were cooled at room temperature inside of the reactor. Then, the samples were exposed to the oxidation reactor for 4, 8, 12 and 16 hours at a constant temperature of 850 ^{0}C. After the oxidation the samples were washed with de-ionized water. As was mentioned above, the samples were characterized and weighed using a Fisher Scientific A-160 mass balance to ± 0. 00001 grams, before and after each process

4.2 Diamond treatment with platinum

After the untreated diamond samples were exposed in the OXR is sulfuric acid decomposition products for a period time of 4 hours at 850 ^{0}C, the diamond samples were disintegrated at the end of this period time, as consequence of the corrosion. The higher diamond corrosion occurred, as a result of the concentration of oxygen free radicals created in the decomposition of sulfur trioxide in sulfur dioxide[37]. One of the products of the corrosion of diamond is the formation of carbon monoxide, because the oxygen free radicals tend to break the carbon sp^3 bonds in the diamond[3].

4.2.1 Annealing in hydrogen atmosphere.

The first part of the research is to present the results on the diffusion of platinum on diamond type II/A plates using the modified FEDOA in the annealing process. The annealing process used a hydrogen atmosphere (Figure 4.2). As was mentioned, the samples were characterized before and after each process by Raman spectroscopy, SEM, EDS, I-V, AFT and UV-Vis spectroscopy techniques were used to characterize the samples.

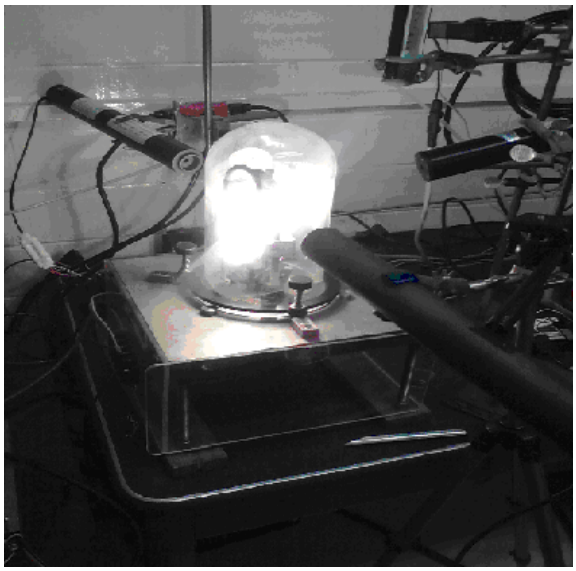

Figure 4.2 Annealed process

4.2.2 Discussion

Raman analysis was performed using a Delta Nu nuscope micro Raman system. Figure 4.3 shows the Raman spectrum taken for samples one, two and three. Sample one was untreated (blue color). The results reveal that the samples exhibit a vibration peak at 1331.29 cm^{-1}, which is characteristic of diamond. The intensity of the peak was low for the spectrum with annealing (sample three, red) because the sample was partly covered with platinum, which absorbed the laser light[38], as a result of the annealing conditions. The intensity of the peak was 480 cm^{-1} which corresponds to nitrogen as a result of the sputtering conditions.

In Raman spectroscopy the intensity of peak moved from 1331.29 cm^{-1} to 1366.48 cm^{-1}. This peak shift is characteristic of the annealing at high temperatures, related to Pt/diamond[39].

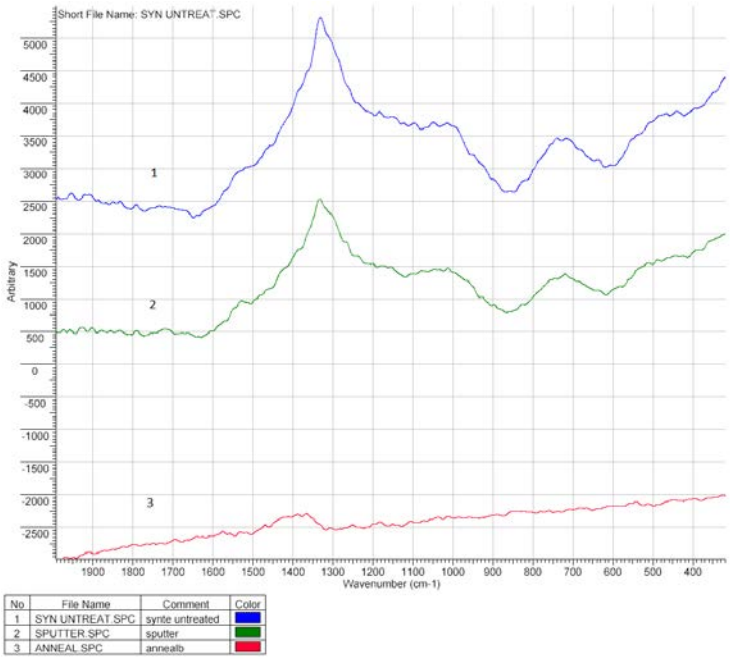

Figure 4.3 Raman spectrum of untreated (sample 1, peak 1331.29cm^{-1}), sputter (sample 2, peak 133.05cm^{-1}) and annealing (sample 3, peak 1366.48 cm^{-1}) diamond samples.

Figure 4.4 shows the Raman spectrum for sample three after four hours in the OXR. The results show that the peak move from 1366.48 cm^{-1} to 1381 cm^{-1} as a result of the environmental conditions in the oxidation reactor.

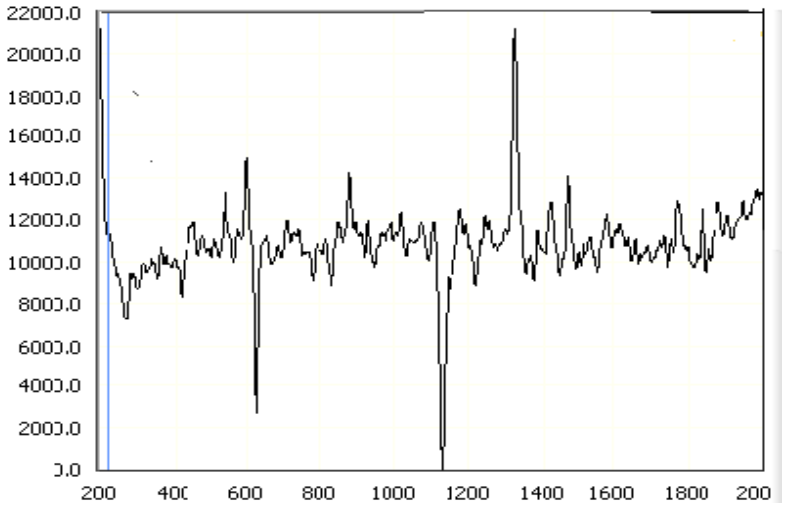

Figure 4.4 Raman spectrum of diamond sample 3 after 4 in OXR

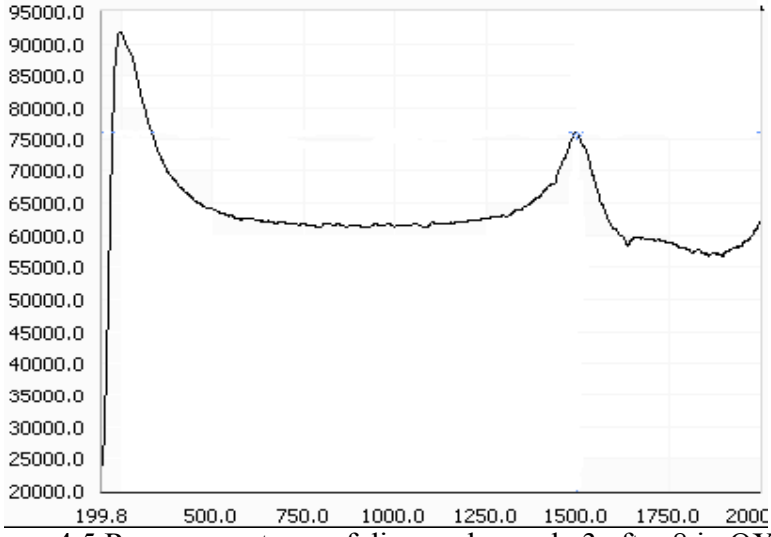

Figure 4.5 Raman spectrum of diamond sample 3 after 8 in OXR.

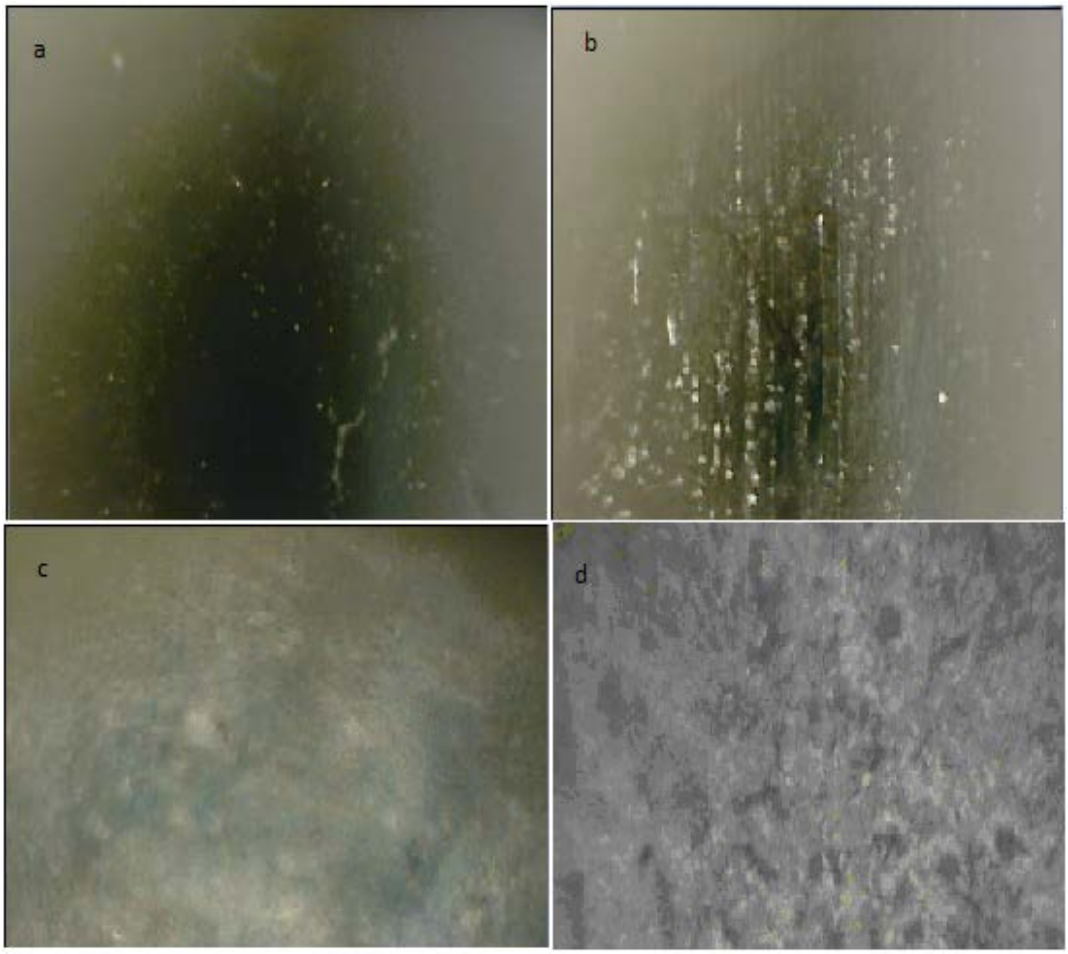

Figure 4.6 Micrograph of diamond samples in each process, selected for the Raman spectra's. (a) Sample untreated, (b) sample treated, (c) sample with annealing, (d) sample after the OXR (4 hours).

The UV-VIS results (Figure 4.7) show that the slope for sample 3 with annealing is smoother, confirming the Raman spectroscopy results. The annealing process reduced the absorption spectrum as a result of the uniform distribution of Pt in the diamond surface[40].

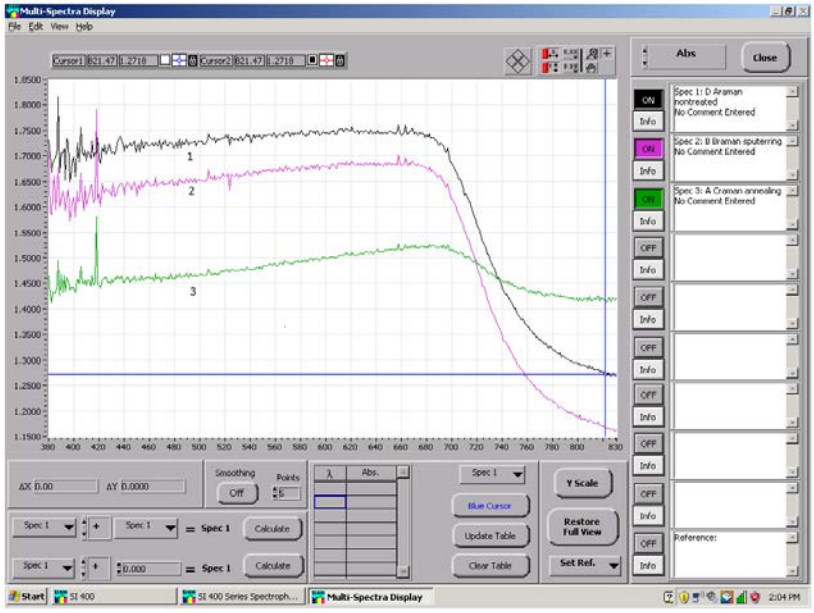

Figure 4.7 UV-Vis for the untreated (1), the sputtering (2), and the annealing (3) diamond samples

Figures 4.8, 4.9, a nd 4.10 show the results obtained from the IV_QDLTS. The samples reveal a linear response in both cases after sputtering and annealing from nano-ampere (nA) to mili-ampere (mA) and the voltage between ± 10 volts (Figs 4.8 and 4.9). The decrease of the current and the voltage (QDLTS) between after and before the annealing is the result of diffusion of Pt in diamond[11], and the current decrease after the annealing process as a result of a change in the surface area, size and shapes of platinum particles[39,40]. Each one is affected by the environmental conditions of the annealing process.

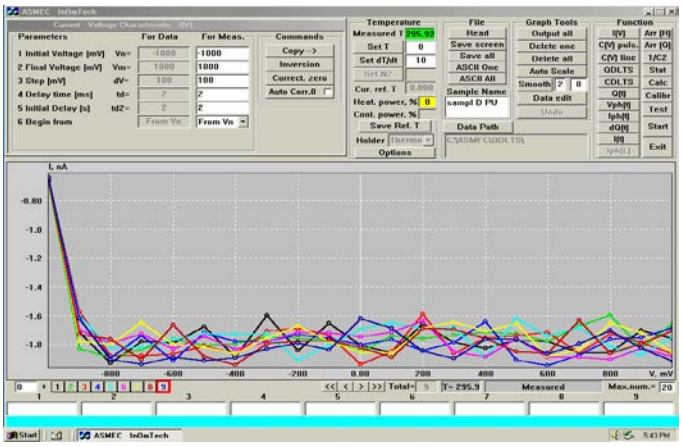

Figure 4.8 Sample 1 (untreated diamond)

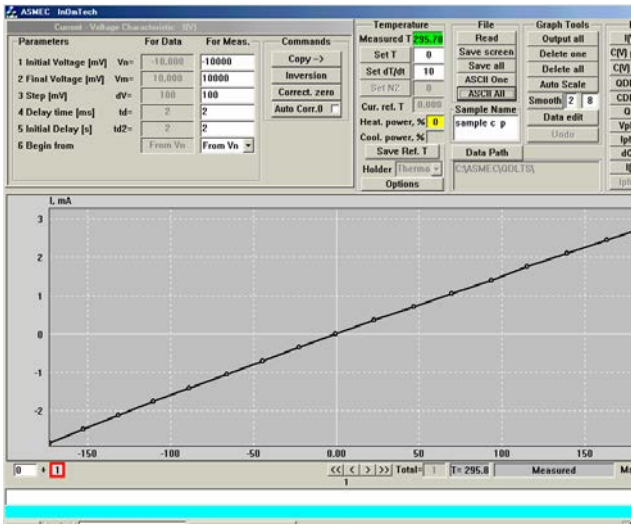

Figure 4.9 Sample 2 (diamond with sputtering)

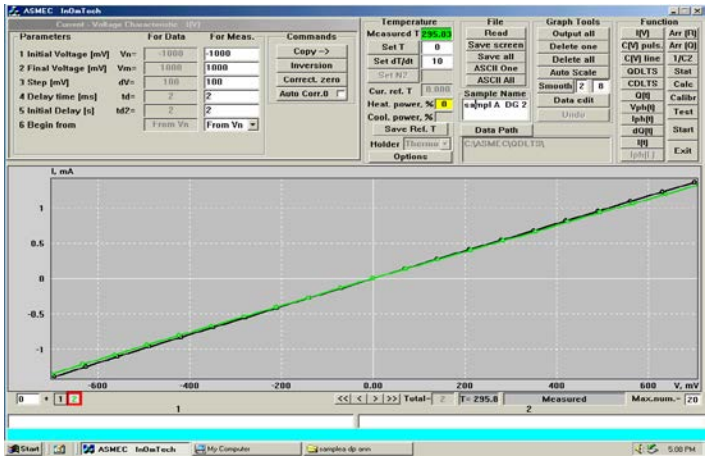

Figure 4.10 Sample 3 (sputtering and annealing)

The samples were inspected after each process using a scanning electron (SEM) microscope. An increase of the surface roughness was observed (Figures 4.110b-d), as a result of the annealing and oxidation processes. Some light spots were observed after the annealing and oxidation processes. The EDS identified the light spots as platinum (Figures 4.13, 4.14).

Figures 4.12 through 4.15 show the EDS analysis of untreated and treated samples. Figure 4.11 show the EDS analysis of the untreated sample. The EDS did not identify any impurity in the diamond sample. Figure 4.13 show the EDS analysis of the treated sample (sputtering) and the platinum was identified. The presence of oxygen is a result of the environmental conditions of the sputtering.

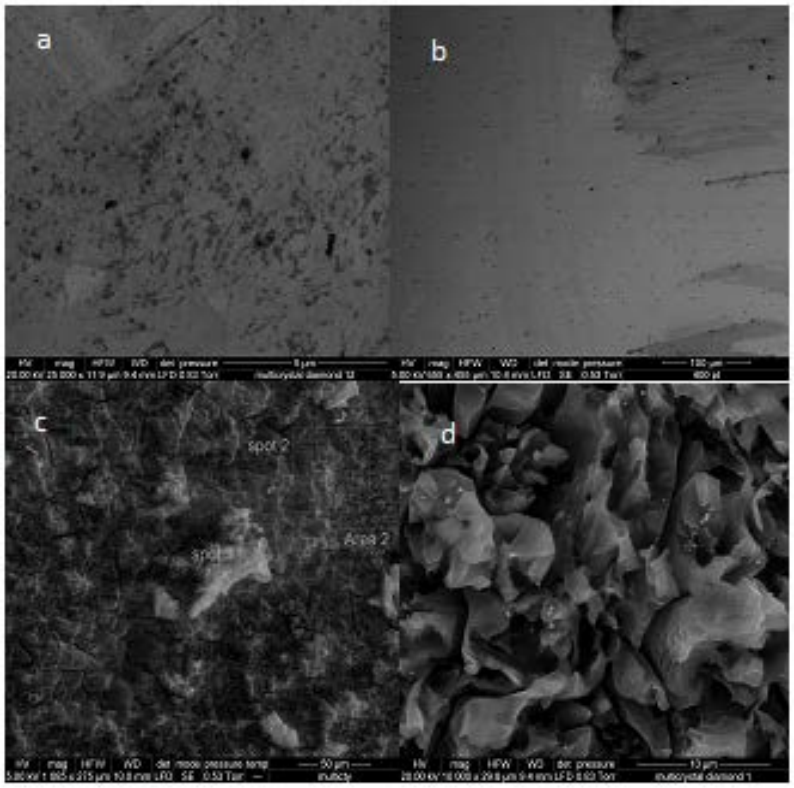

Figure 4.11.SEM micrographs of the: untreated (a), with sputtering (b), after annealing (c), after oxidation (d) diamond samples

Figures 4.14 and 4.15 show the EDS analysis after annealing and oxidation processes, respectively. Impurities detected on the samples after each process were the result of the environmental conditions. It was also found that the concentration of impurities on the same sample changed from one point to another as showed by EDS. The intensity of platinum after the annealing (Figure 4.14), decrease as the result of the diffusion on diamond, and also as a consequence of the impurities present in the reactor. The platinum identified after the oxidation process (Figure 4.15), reveals that the oxidation process created a homogenous coating on the samples. The EDS analysis showed that the intensity of Pt increased on some parts of the sample as a result of the formation of platinum cluster (Figures 4.14, 4.15). The formation of the clusters is a result of the high temperatures in the annealing process [35].

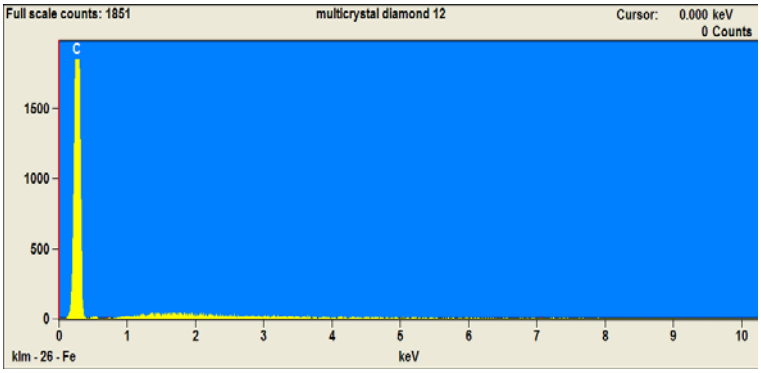

Figure 4.12.EDS analysis of the untreated diamond sample.

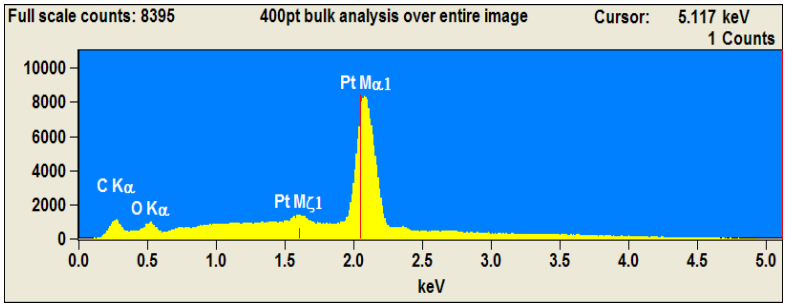

Figure 4.13 EDS analysis of treated diamond sample (after sputtering)

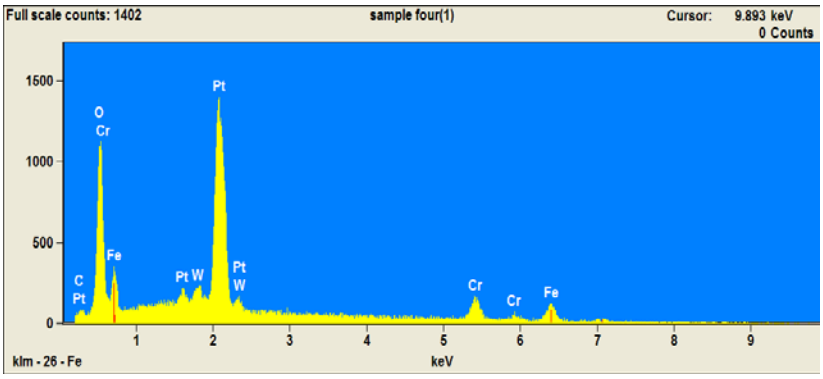

Figure 4.14 EDS analysis of diamond sample after annealing

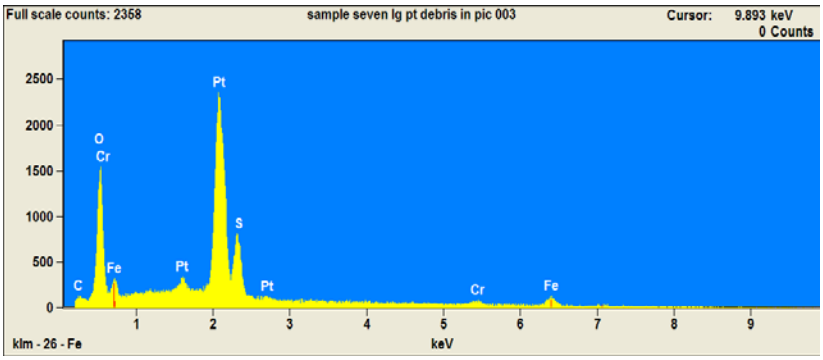

Figure 4.15 EDS analysis of diamond sample after oxidation process.

The samples were inspected optically after each process using the "Atomic force microscopy" (AFM-Vecco). The AFM was operated in "tapping mode" and the scanning probe microscope (spm), probe used was antimony (n) doped silicon with a force constant of 20-80 N/m and a frequency of 312-359 KHz. Surface analysis using AFM confirmed an increase in surface roughness in the samples after the annealing and oxidation process (Figure 4.15), as observed in the SEM.

The formation of Pt clusters after the annealing, observed in the SEM were also confirmed by AFM, giving rise to significant porosity and enhance surface area[42]. The

formations of clusters were the result of the environmental conditions in the sputtering process[41].

The present of defects and formation of impurities in the surface can be observed with the AFM as show in Figure 4.16. Table 4.1 summarizes the results of diamond samples treated with platinum, after different temperatures and gases in the annealing process.

Table 4.1 Diamond samples treated with Platinum.

Sample	Annealing: (^{0}C/h) temperature/time	Environment	Weight/before oxidation (gr)	Oxidation: (^{0}C/h) temperature/time	Weight /after oxidation (gr)
Sample 1	500/8	Helium	0.20195	810/8	0.20190 a
				822/16	0.20187 b
Sample 2	600/8	Helium	0.33468	810/8	0.33468
				822/16	0.33462 b
Sample 3	500/8	Hydrogen	0.32316	810/8	0.32312
				822/16	0.32316
Sample 4	600/8	Hydrogen	0.33328	810/8	0.33325
				822/16	0.33327
Sample 5	700/8	Hydrogen	0.33451	822/8	0.33448
				822/16	0.33450
Sample 5	500/8	Argon	0.33310	810/8	0.33299 a
				822/16	0.33105 b
Sample 6	700/8	Argon	.33226	810/8	0.33220
				822/16	0.33200 c
Sample 7	900/6	Argon			

a, b: The samples lost mass after 8 and 16 hour, also after 24 hours the samples was disintegrated and: c: The sample continued to lose mass after temperature was increased.

4.3 Stainless steel treatment with platinum

The second objective of this research was to investigate the performance of different materials vs. modified materials under a simulated acid decomposition. As a

result of this investigation, stainless steel 404 and 304 were treated with platinum and iridium to improved resistance to corrosion in harsh environments, like the case of the decomposition of sulfuric acid decomposition. Stainless steel samples with the same shape (1 cm^2 by 0.04572 mm thick) were selected. The cleaning process, treatment and characterization were described in the previous sections.

After the samples were clean, Pt was sputtered process on both sides of the sample, 50-55 minutes each side. The sputtering process was performed in a Denton vacuum, LLC, Desk IV sputter with an argon atmosphere. The thickness of the deposition was 1-1.2 KÅ and the target was platinum.

After the sputtering, the samples went through an annealing process. A modified version of FEDOA[3] was used to improve the annealing process at higher temperature and vacuum. The temperature and vacuum were 500-800^oC and 10x4 Pa, respectively for 3- 6 hours in a hydrogen atmosphere. After the annealing process, the samples were cooled at room temperature inside of the reactor. After cooled, the samples were exposed to the oxidation reactor for 4, 8 and 12 hours at a constant temperature of 850^0C. As was mentioned above, the samples were characterized and weighted.

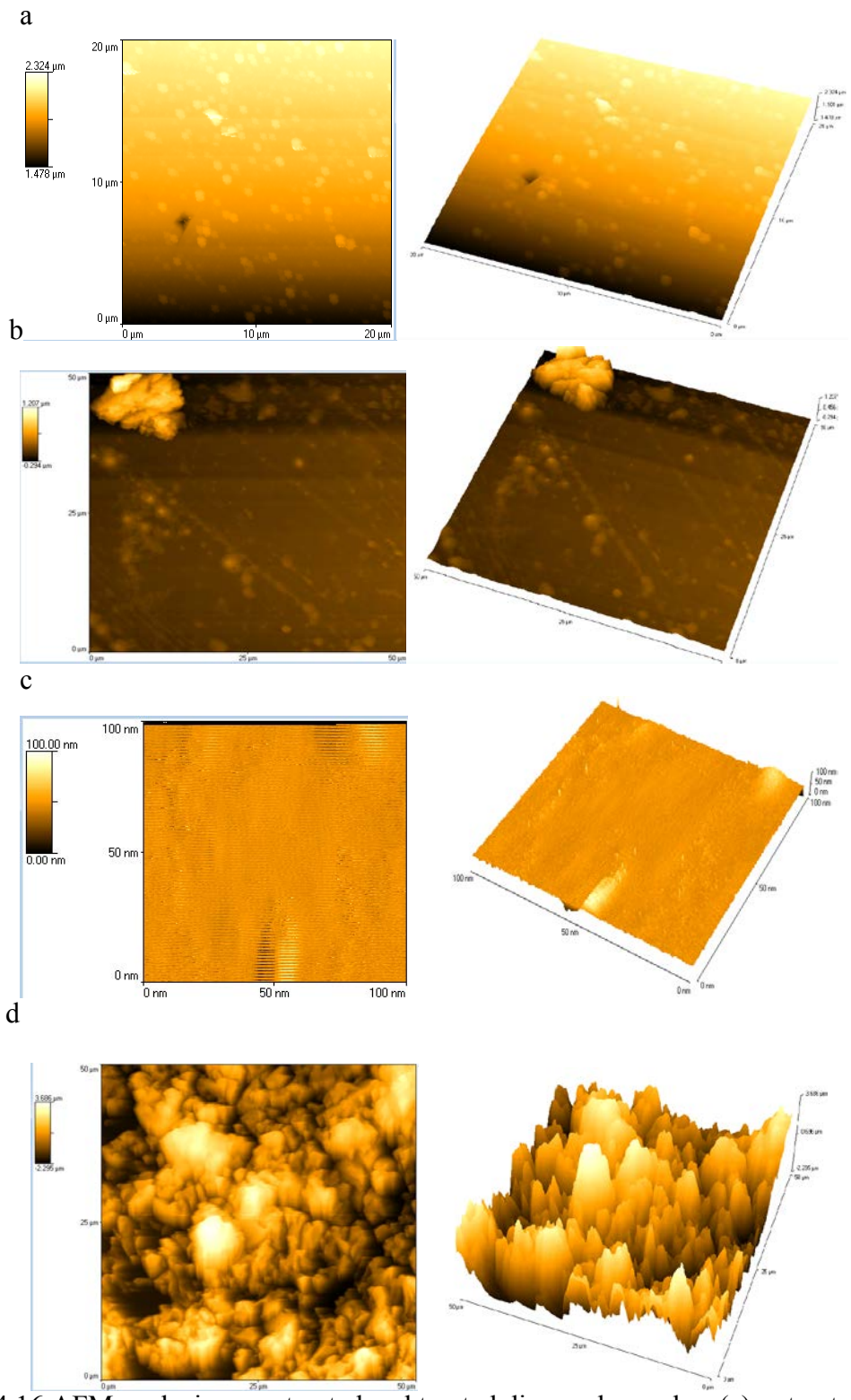

Figure 4.16 AFM analysis on untreated and treated diamond samples: (a) untreated, (b) after SP, (c) annealing and (d) after OXR

4.3.1 **Annealing in hydrogen atmosphere**

The second part of the research is to present the results on the diffusion and treatment of platinum on stainless steel type 304 and 403 plates using the modified FEDOA in the annealing process. The annealing process used a hydrogen atmosphere (Figure 4.2). As was mentioned in the section 4.2, the samples were characterized before and after each process. Raman spectroscopy, SEM, EDS, I-V, AFT and UV-Vis spectroscopy techniques were used to characterize the samples.

4.3.2 Discussion

Raman analysis was performed using a Delta Nu nuscope micro Raman system. In the figure 4.17 shows the Raman spectrum taken for the untreated sample. The results show a vibration peaks at 670 cm^{-1}, 1050 cm^{-1}, are related with $NiFe_2O_4$ and $NiCr_2O_4$. Additional peaks were observed at 1470 cm^{-1}, related with $NiFe_2O_4$ respectively.[41]The intensity of peaks observed and wavelength depended of the stainless steel composition[34].

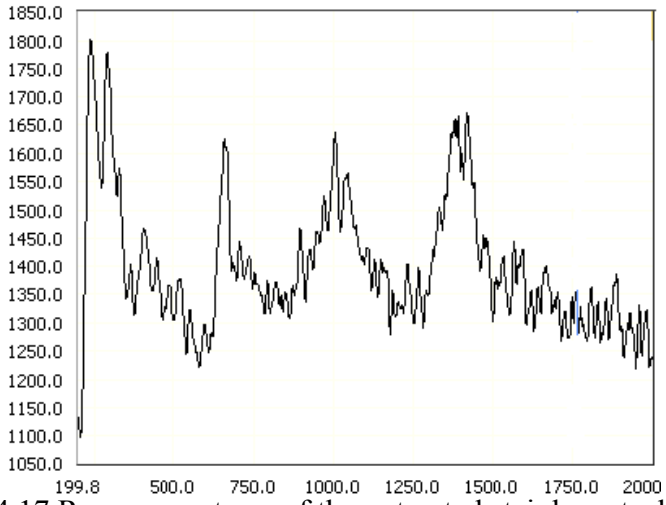

Figure 4.17 Raman spectrum of the untreated stainless steel sample

After the sample was treated with platinum (Figure 4.18), the Raman spectrum showed that the peaks intensities at 650 cm^{-1}, 1050 cm^{-1} and 1470 cm^{-1} were low because the sample was covered with platinum, which absorbed the laser light. The same result was observed in the case of diamond treated with platinum.

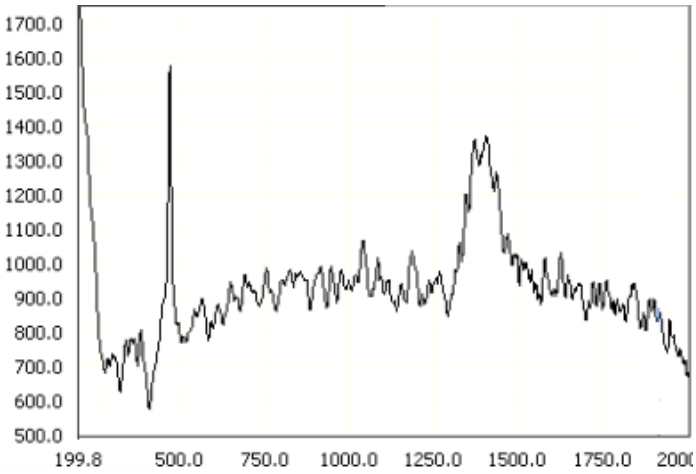

Figure 4.18 Raman spectrum for the stainless steel sample treated with platinum.

The peaks described and identified in the Figures 4.17 and 4.18 related with stainless steel and platinum decreased its intensity, as a result of the uniform distribution of platinum in the stainless steel surface at high temperatures (Figure 4.19). The results show that the peak move from 500 cm^{-1} to 540 cm^{-1} as results of the environmental conditions in the annealing process. The peaks shift was also observed in the case of Pt/diamond, which is characteristic for platinum, in cases where the annealing process is at high temperatures[38].

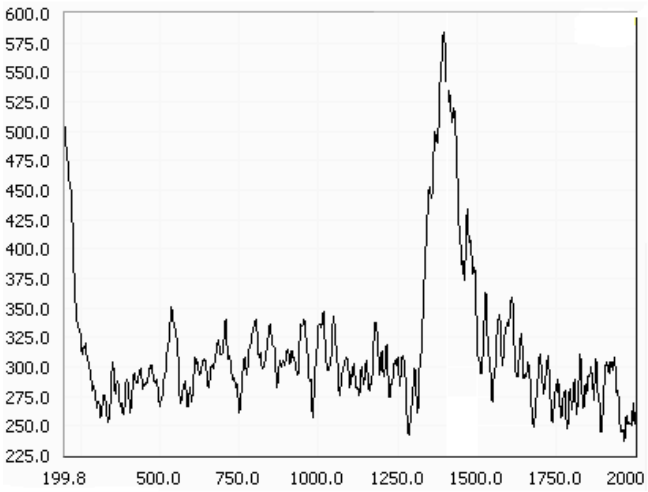

Figure 4.19 Raman spectrum for the stainless steel sample treated after annealing process.

Figure 4.20 shows the Raman spectrum for sample after four hours in the OXR. The results show that the peak move from 540 cm^{-1} to 500 cm^{-1} as results of the conditions in the OXR, also the intensity of the peaks was increases as results of the formation of Pt cluster at high temperatures. The formation of clusters was observed too, in the annealing process in a hydrogen atmosphere, in the case of Pt/diamond[38] process described in previous sections.

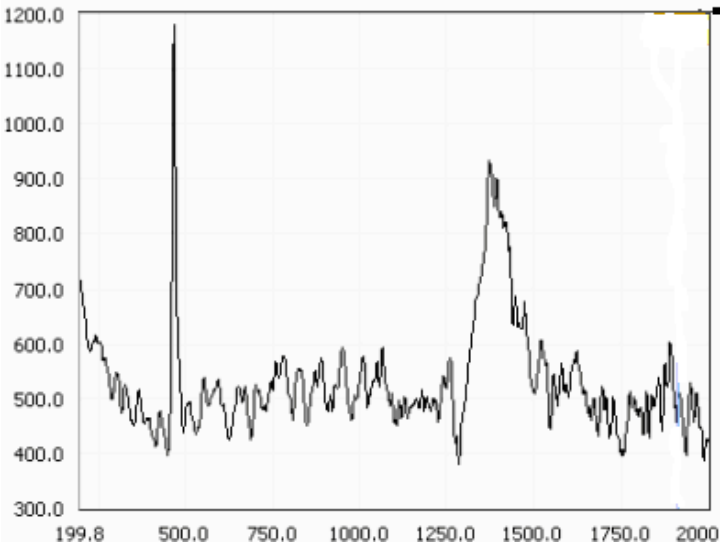

Figure 4.20 Raman spectrum for stainless steel sample treated after 4 hours in the OXR

Figure 4.21 show a micrograph of the stainless steel in each process, after the annealing process, the sample surface start to change from the smooth to rough as result of the formation of impurities and Pt cluster on the stainless steel. The formations of impurities are the results of environmental conditions in the annealing and oxidation process.

The UV-Vis results (Figures 4.22 and 4.23) show that the annealing process reduced the absorption spectrum as a result of the uniform distribution of Pt in the stainless steel, as observed in the Raman spectroscopy results.

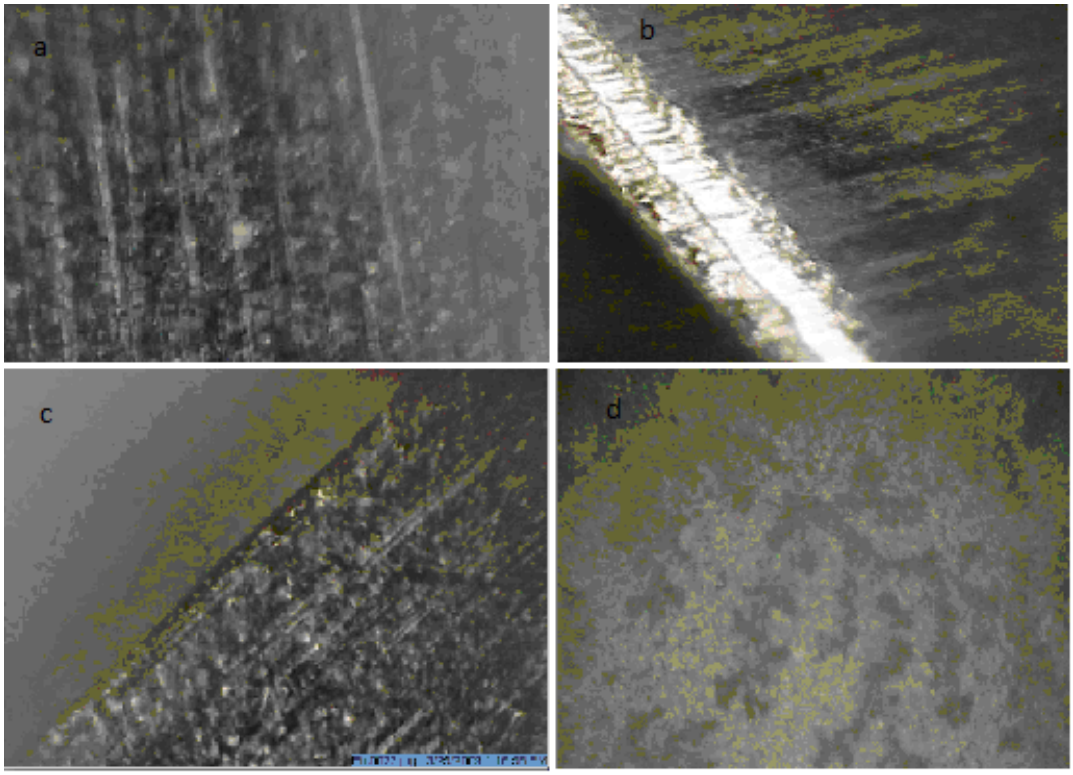

Figure 4.21 Micrograph of the stainless steel samples in each process, selected for the Raman spectroscopy. (a) Sample untreated, (b) sample treated, (c) sample with annealing, (d) sample after the OXR (4 hours)

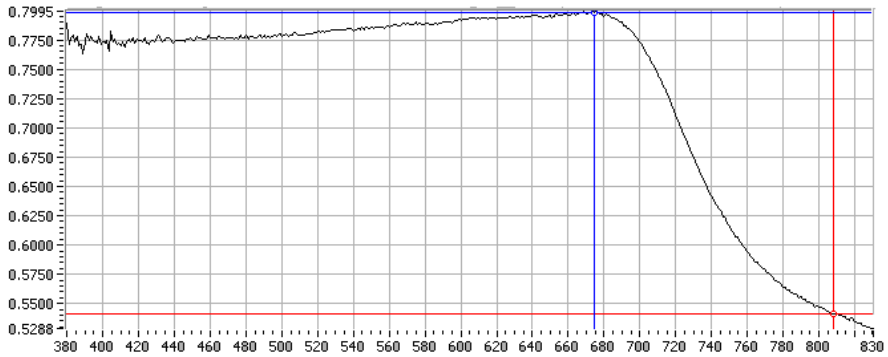

Figure 4.22 UV-VIS for stainless steel sample treated after sputtering process

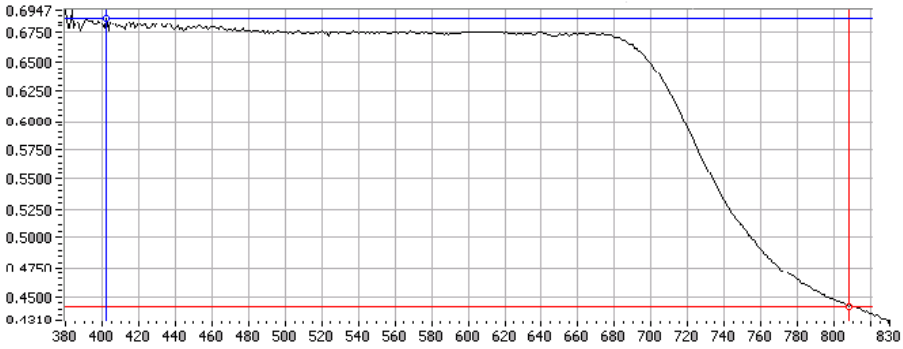

Figure 4.23 UV-VIS for the stainless steel sample treated after annealing process

Figures 4.24, 4.25, 4.26 show the results from IV_QDLTS. The samples showed linear response, in the cases after sputtering and annealing between ± 200 mA and ± 2V (Figures 4.25 and 4.26). The increase of the current and voltage after the annealing (Figure 4.26) is the result of a uniform surface and changes in the size and shapes of platinum, as a consequence of the high temperature and the gas used in the annealing process[19].

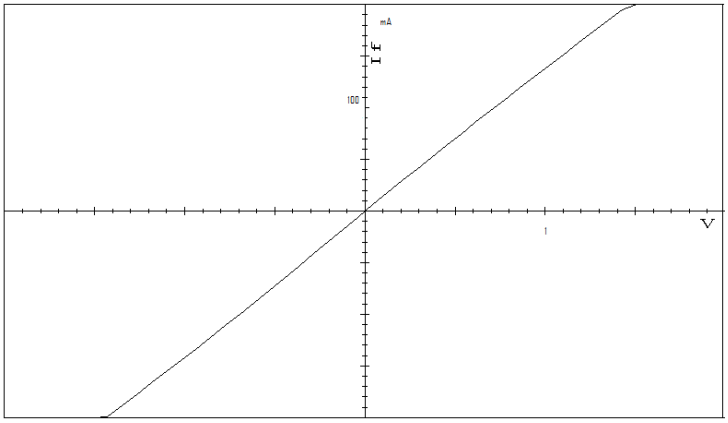

Figure 4.24 Stainless steel untreated

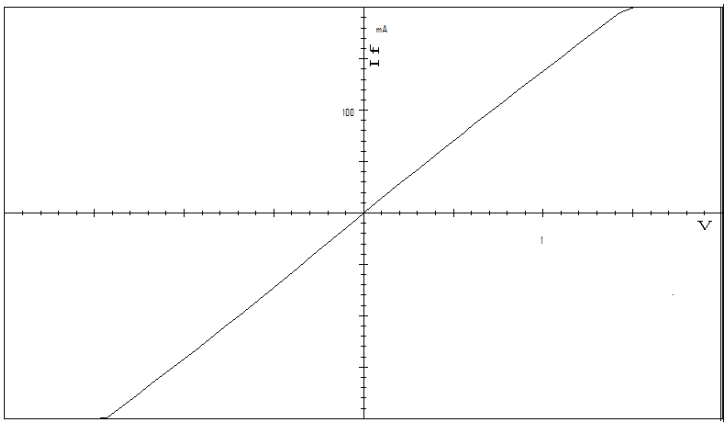

Figure 4.25 Stainless steel treated with platinum

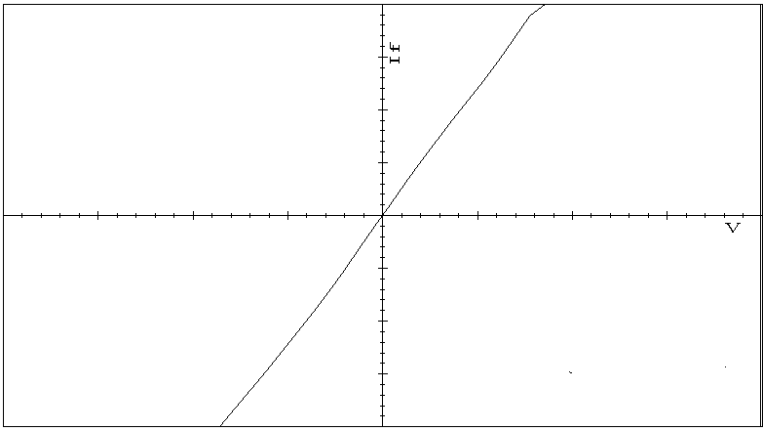

Figure 4.26 Stainless steel treated after annealing process

In previous analyses, a surface changes in some of the samples from smooth to roughness was identified. For this reason, the samples were inspected using SEM.

An increase of the surface roughness was observed (Figure 4.27 a-d), as a result of the annealing and oxidation processes in the case of stainless steel samples treated with platinum.[40].

The Figure 4.27b shows that the sputtering process was not uniform, consequently dark spots were observed. The EDS analyses (Figure 4.28), show that the concentration of platinum in these spots is low, in compared with the bright spots. Also, the concentration of platinum and impurities on the same sample changed from one point to another, as was identified by DES (Figure 4.28).

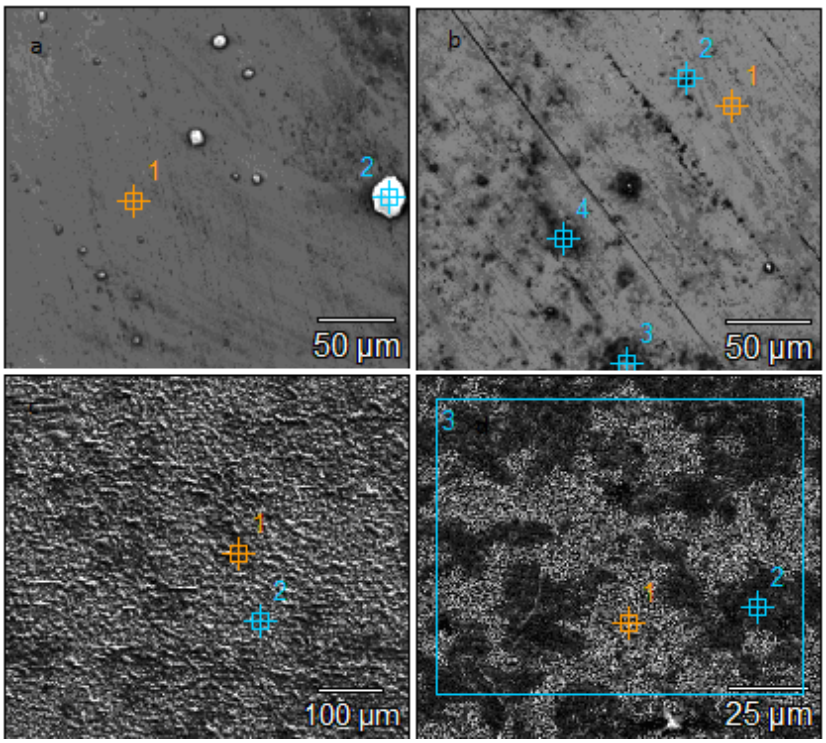

Figure 4.27 SEM images of: untreated (a), with sputtering (b), after annealing (c), after oxidation (d) stainless steel samples

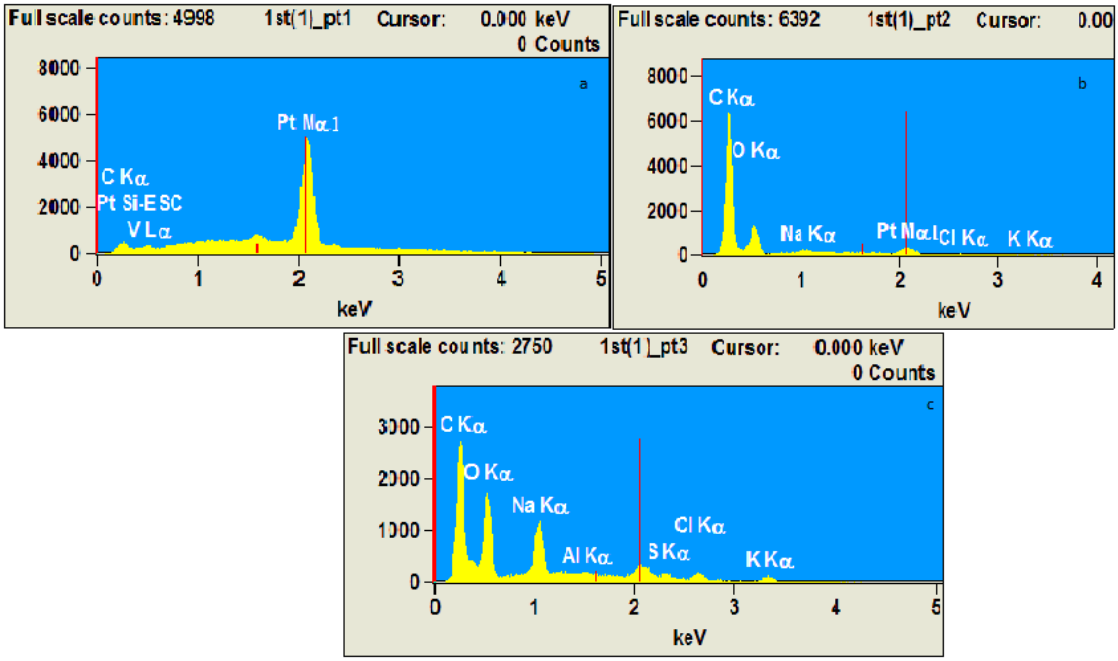

Figure 4.28 EDS analysis of stainless steel sample in different points after sputtering process

Figures 4.29 and 4.30 show the EDS analysis after annealing and oxidation processes. As was mentioned before, the impurities on the samples were the result of the environmental conditions.

EDS analysis showed that the intensity of the platinum after the annealing process (Figure 4.29) increased as a result of the cluster formation platinum[44]. The clusters formations are the result of environmental conditions in the annealing process (Table 4.2).

Figure 4.30 shows that the concentration of platinum after the oxidation process was constant, due to the homogeneous coating on the samples (Table 4.2).

The SEM analysis results not show any corrosion after the oxidation process, the dark areas on the samples are the result of the formation of impurities[11, 29] (Figure 4.27d).

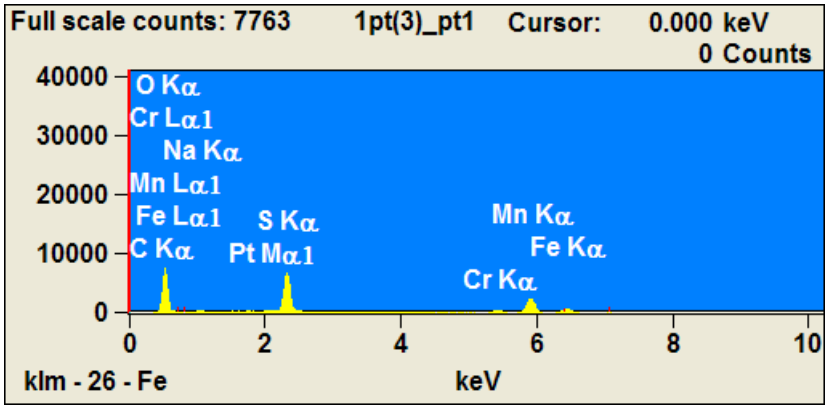

Figure 4.29 EDS analysis of stainless steel after annealing

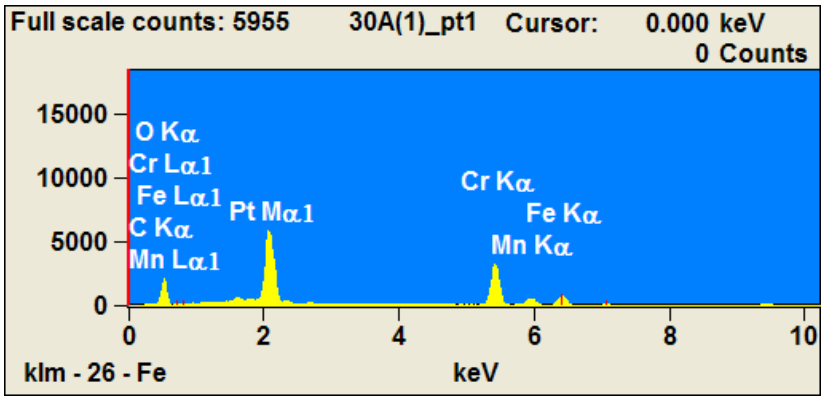

Figure 4.30 EDS analysis of stainless steel after oxidation process

When the samples were not subjected to the annealing process, the formation of cluster, crevice and pit was higher in the oxidation process, after four to twelve hours (Figure 4.31). After twelve hours, it was observed minimal corrosion in the stainless steel samples, also the formation of clusters was irregular in size and geometry[47]. The EDS analyses reveal that the clusters are formation of platinum (Figure 4.32).

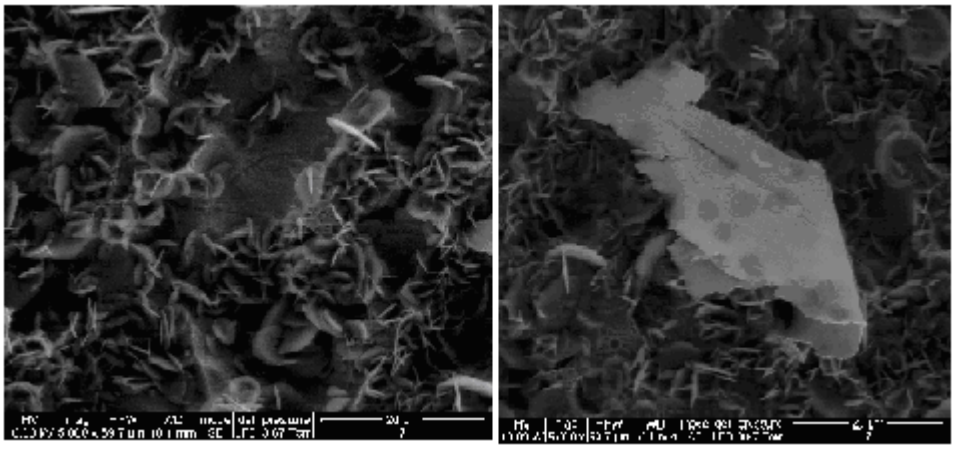

Figure 4.31 SEM images of stainless steel samples treated with platinum, without annealing after 12 hours in OXR

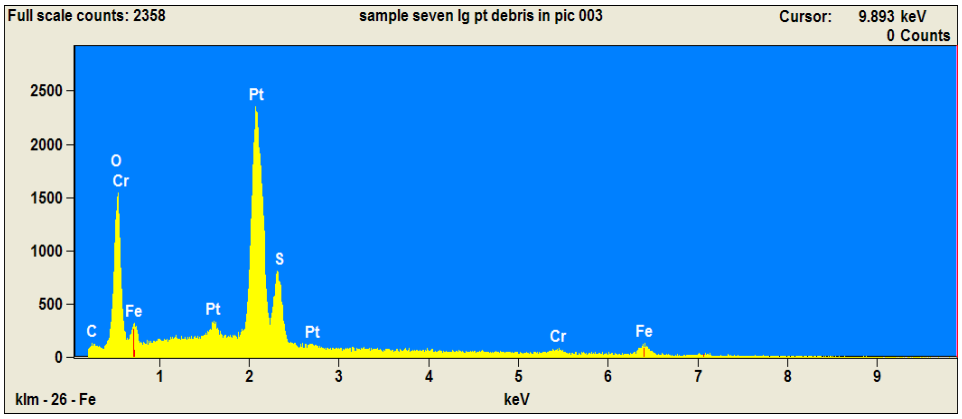

Figure 4.32 EDS analysis of stainless steel samples treated with platinum, without annealing after 12 hours in OXR

Optical inspection and surface analysis was performed using AFM. Surface analysis using AFM confirmed an increase in surface roughness in the samples after the annealing and oxidation process (Figure 4.33c-d), as observed in the SEM. Also the AFM confirmed the presence of imperfections on the surface of untreated samples (Figure 4.33a).

The formation of Pt clusters, pit and crevice after the annealing, observed in the SEM were also confirmed by AFM (figure 4.33a-b), giving rise to significant porosity and deterioration of the surface of samples [42]. The formations of clusters were the result of the environmental conditions in the sputtering process and annealing process.[41]

The AFM analysis concur that the increased in the surface roughness was higher in the OXR (Figure 4.33d) than in previous processes (sputtering, annealing), as a result of the environment conditions and high formation of impurities (Figure 4.26). Table 4.2 summarizes the results of stainless steel samples treated with platinum, after different temperatures and gases in the annealing process. Besides the exposure time of samples in the oxidation reactor.

Table 4.2 Stainless steel treated with Platinum.

Sample	Annealing:(^{0}C/h) temperature/time	Environment	Weight/before oxidation (gr)	Oxidation:(^{0}C/h) temperature/time	Weight /after oxidation (gr)
Sample 10	500/2	Hydrogen	0.33579	803/4	0.33543 a
Sample 11	(600-800)/3	Hydrogen	0.28944	815/4	0.28940
Sample 12(6.3)	700/3	Hydrogen	0.35180	810/8H	0.35179
Sample 13(30)	800/3	Hydrogen	0.0.24162	820/12	024220
Sample 14(31)	500/2	Helium	0.50896	803/4	0.50763 a
Sample 15(161)	700/3	Helium	0.32246	815/4	0.32201 a
Sample 16	800/3	Helium	0.33411	810/8	0.33408
Sample 17	900/3	Helium	0.33410	820/12	0.33413
Sample 18(80)	700/3	Argon	0.28780	815/4	0.28531 a
Sample 19(81)	900/3	Argon	0.33422	810/4	0.33402

(a) The sample lost mass.

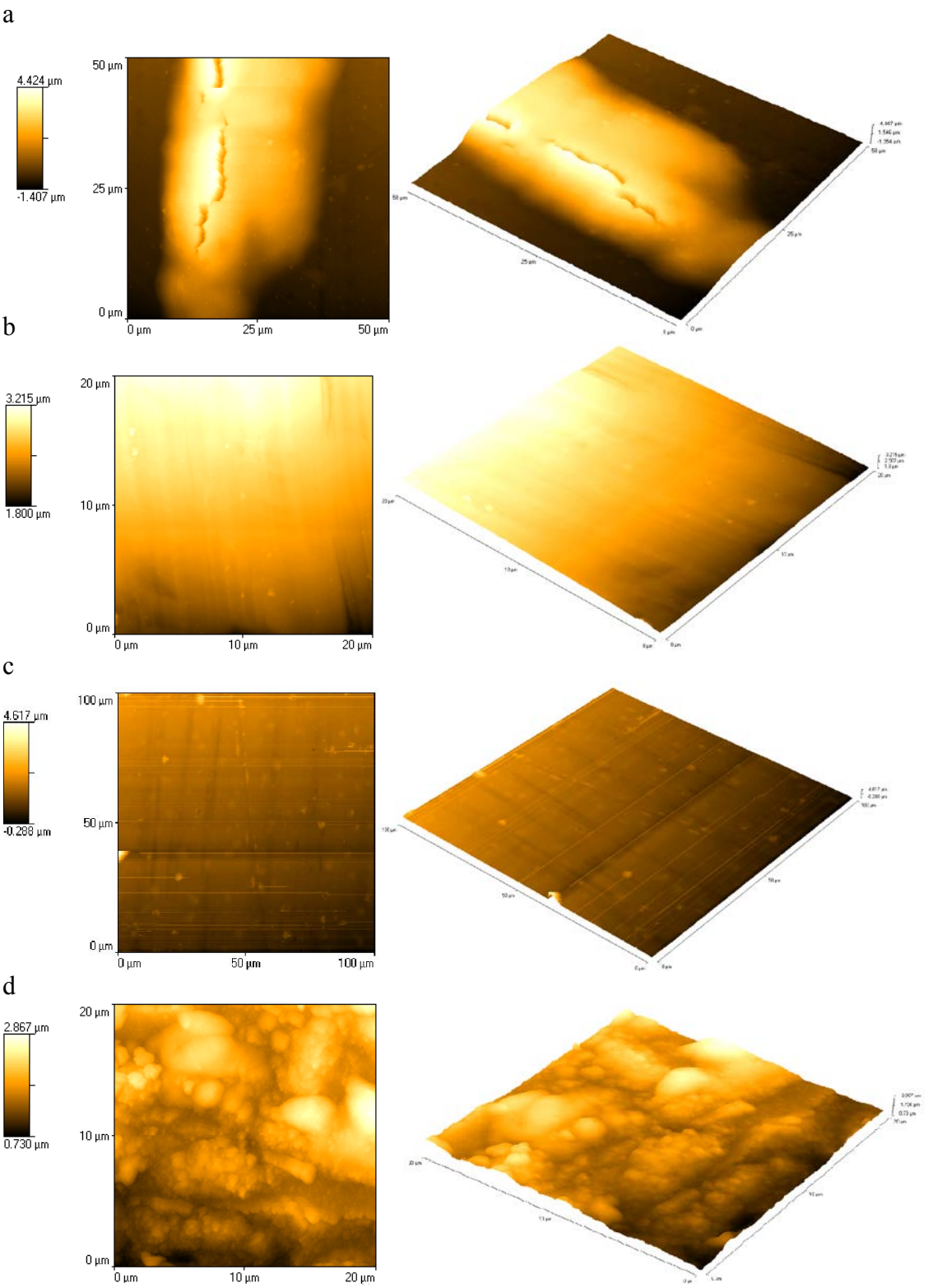

Figure 4.33 AFM analysis on untreated and treated stainless steel samples: (a) untreated, (b) after SP, (c) annealing and (d) after OXR.

4.4 Stainless steel treated with iridium

Stainless steel 404 and 304 samples were treated with iridium, characterized before and after each process, as was described in section 5.3. After, the samples went through an annealing process (A modified version of FEDOA). The temperature and vacuum were 600-1000^{0}C and 10^{-4} Pa, respectively for 4 hours in a hydrogen atmosphere. As was mentioned before (section 5.3) the samples were cooled at room temperature. After the cooled, they were exposed to the oxidation reactor for 4 and 8 hours a constant temperature of 825^{0}C.

4.4.1. Discussion

Figure 4.34 shows the Raman results for the stainless steel treated with iridium. The results show a vibration peak at 500 cm^{-1}, related at IrO_2[46], absorbed in the treatment process. Additional peaks were observed at 1150 cm^{-1} related with $NiFe_2O_4$.

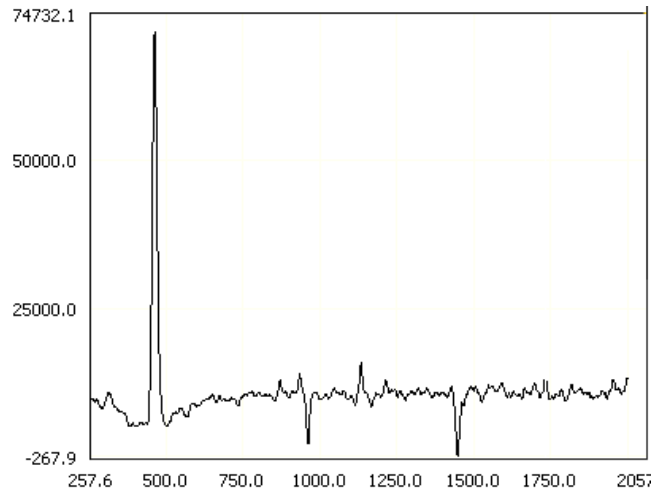

Figure 4.34 Raman spectrum of stainless steel treated with iridium

Figure 4.35 shows the vibration peaks at 490 cm^{-1}, 1330 cm^{-1} and 1660.2 cm^{-1}, related with Ir O_2 and $NiCr_2O_4$, at O_2, respectively. The intensity of the peak at 500 cm^{-1}

decreased as a result of the annealing process at high temperatures in a hydrogen atmosphere. After the annealing process, the sample was tested in the oxidation reactor for 4 hours.

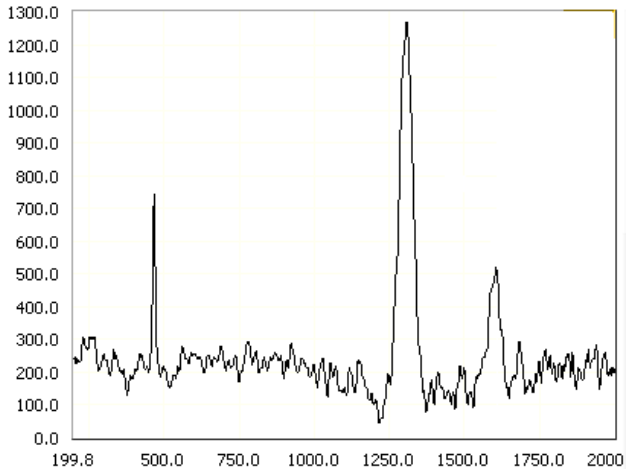

Figure 4.35 Raman spectrum of stainless steel treated with iridium after annealing

Figure 4.36 shoes the Raman spectrum for the sample after four hours in the OXR. The Raman spectrum results show vibration peaks at wavelengths of 490, 715.3, and 1480, are related with IrO_2, $NiCr_2O_4$. The intensity of the peak at 715.3 increased as a result of the uniform coating and also because, at the end of the process, the sample was unprotected. Unidentified additional peaks were observed as a result of the condition in the OXR.

The samples' surface was rough after the treatment with iridium (Figure 4.37 A), as a result of the iridium cluster. After the annealing process the surface changed from rough to smooth (Figure 4.37 B) as a consequence of a uniform coating at high temperatures.

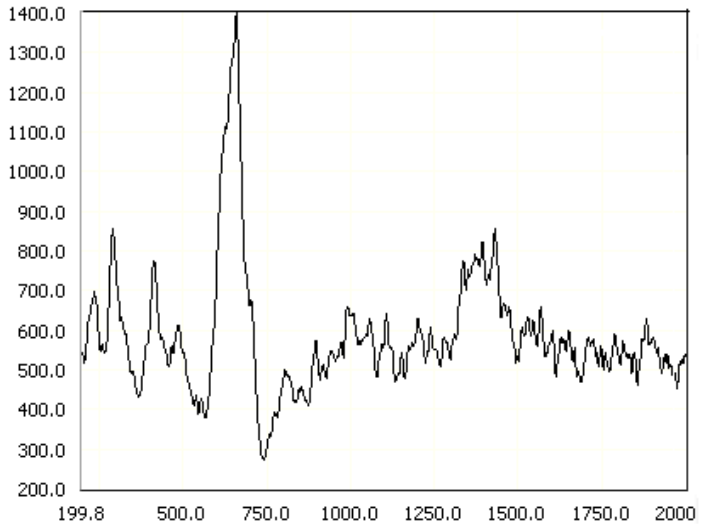

Figure 4.36 Raman spectrum for the stainless steel sample treated with iridium after 4 hours in the OXR.

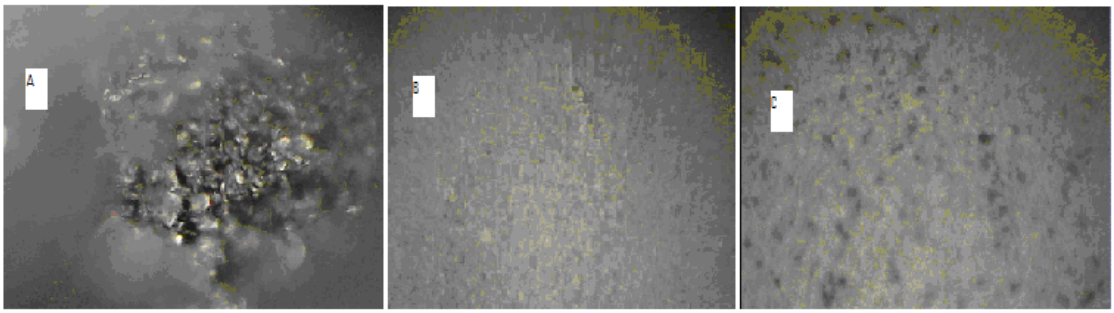

Figure 4.37 Micrographs of the stainless steel samples treated with iridium in each process, selected for the Raman spectroscopy. (A) Sample treated, (B) sample with annealing, (C) sample after the OXR (8 hours)

Figures 4.38 and 4.39 show the results from the IV_QDLTS. After the sputtering and annealing processes, the samples revealed a linear response in both cases, from 200 mA to 1 mA and the voltage from ±3v to ±5v (Figure 4.38 and 4.39), respectively. The decrease of current and increase of voltage (QDLTS) between, after and before the annealing is the result of changes in the size and shapes of iridium, at the presence of impurities, and as a result of the annealing at high temperatures and the gases used.

The IV_QDLTS results of the samples after the oxidation process did not show conduction as a result of the formation of impurities on the surface samples and because samples were uncovered after 16 hours in the OXR.

The formation of iridium clusters after the oxidation process, and the change in the samples' surface from smooth to rough, before and after the oxidation process was confirmed by SEM (Figure 4.40). The increased in the cluster size[47] (Figure 5.40 b) is the result of the presence of impurities and of oxygen free radicals.

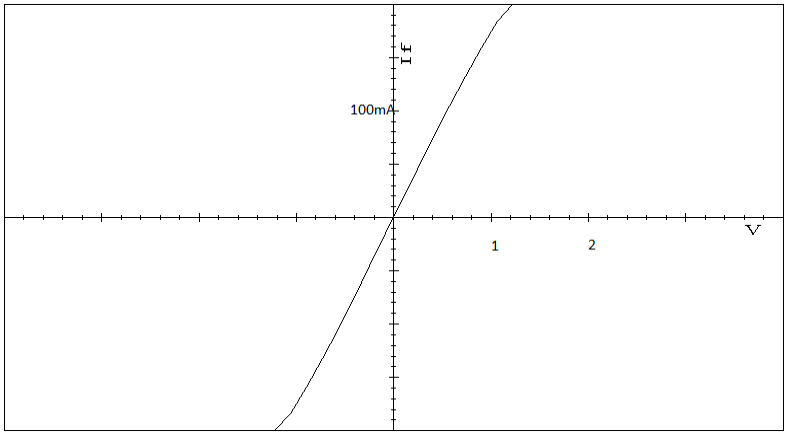

Figure 4.38 Stainless steel treated with iridium

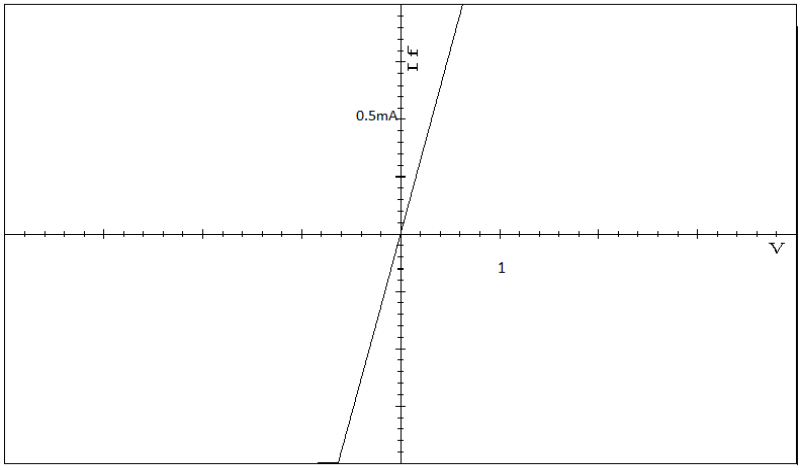

Figure 4.39 Stainless steel treated with iridium after the annealing process

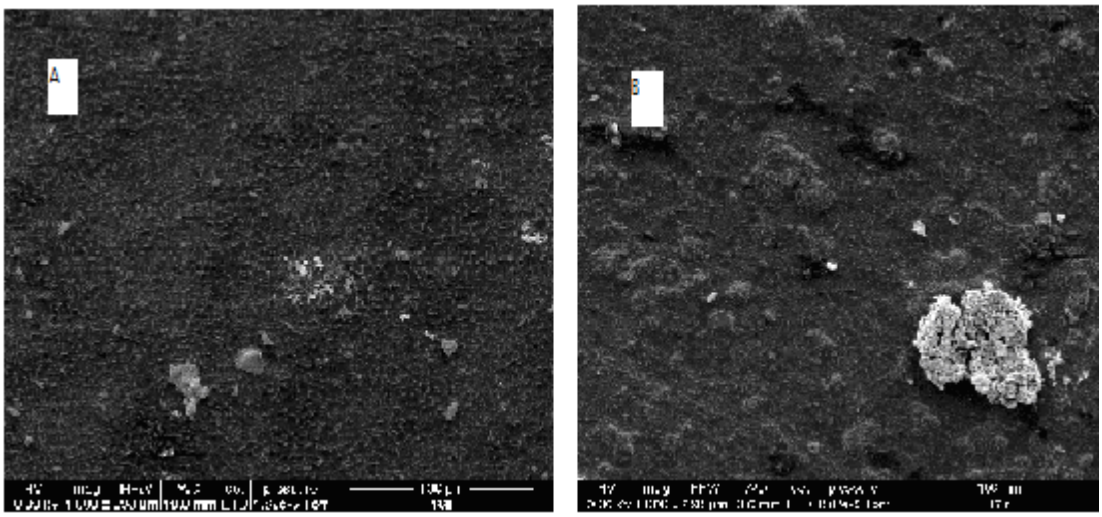

Figure 4.40 SEM images of the stainless steel treated with iridium; (A) after annealing and (B) after oxidation

EDS analysis showed that the intensity of the iridium after the oxidation process (Figure 4.42) decreased as a result of the presence of impurities. Also the concentration of iridium was not constant in the sample as a consequence of the formation of clusters.

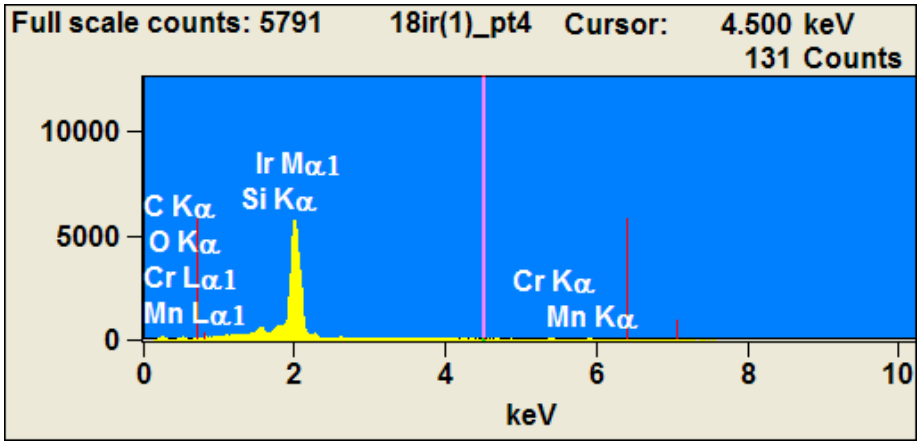

Figure 4.41 EDS analysis of stainless steel treated with iridium after annealing

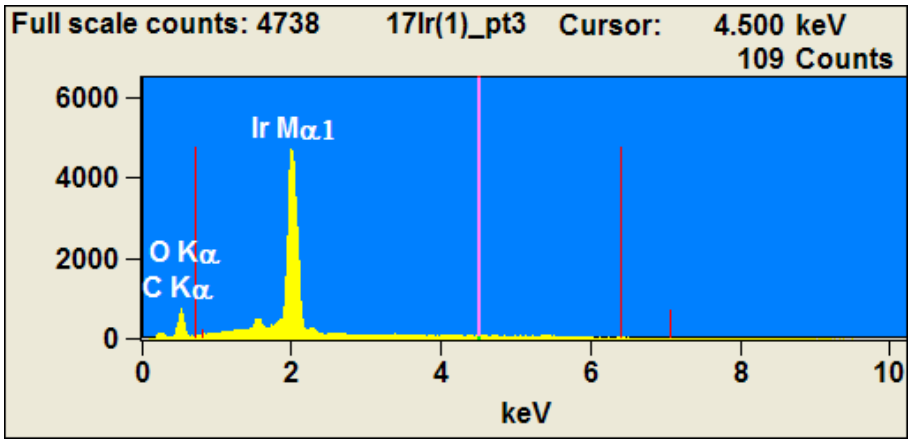

Figure 4.42 EDS analysis of stainless steel with iridium after the oxidation process

AFM confirmed an increased in the surface roughness of the samples after the oxidation process (Figure 4.43 b), as observed at the SEM. Also the AFM confirmed the presence of imperfections on the surface of untreated samples (Figure 4.33a).

The formation of iridium clusters after the annealing, observed in the SEM were also confirmed by AFM (Figure 4.43 a). Also the AFM analysis proved that the size of the clusters increased after the oxidation process (Figure 4.43 b). The increase of size of the clusters is related to the annealing process. The increase of the number and size of the iridium clusters was high, in instances when the annealing temperature was below of 700^0C.

a

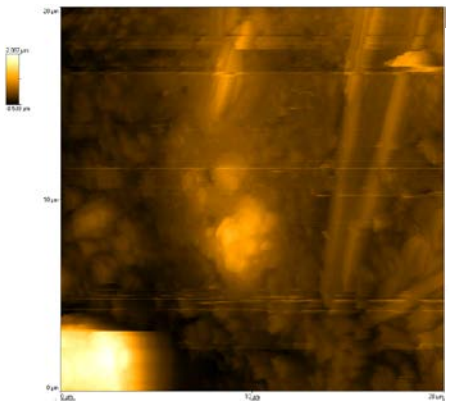

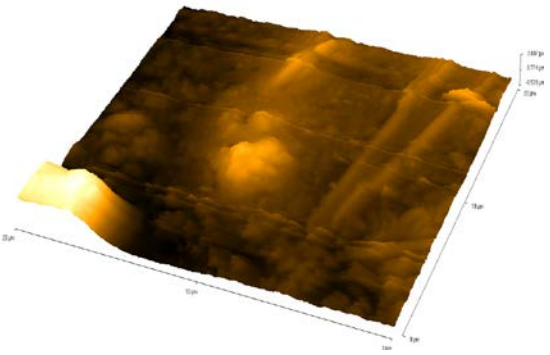

b

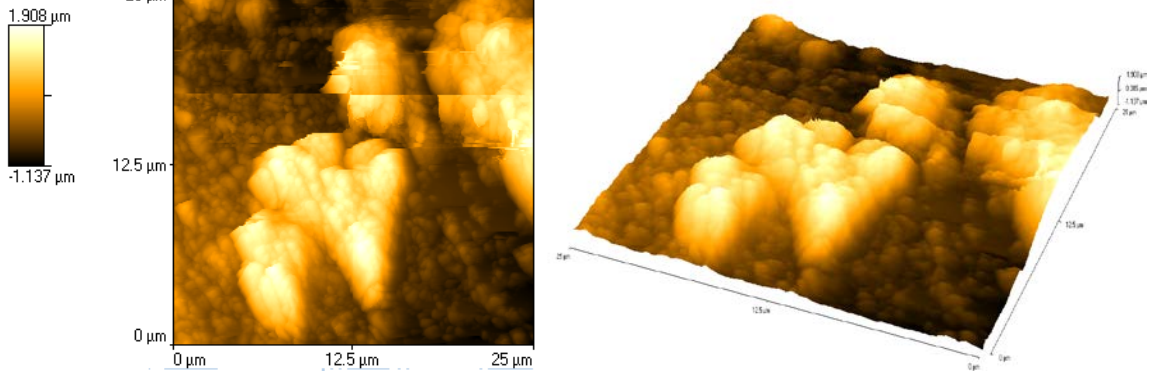

Figure 4.43 AFM analysis on untreated and treated stainless steel samples treated with iridium: (a) annealing and (b) after OXR

The AFM proved that the shape of the iridium clusters (Figure 4.44) was dependant of the type of gas used and the temperature in the annealing process. In the cases where the annealing was at the same temperature, the cluster shapes were dependent of the impurities present in the process.

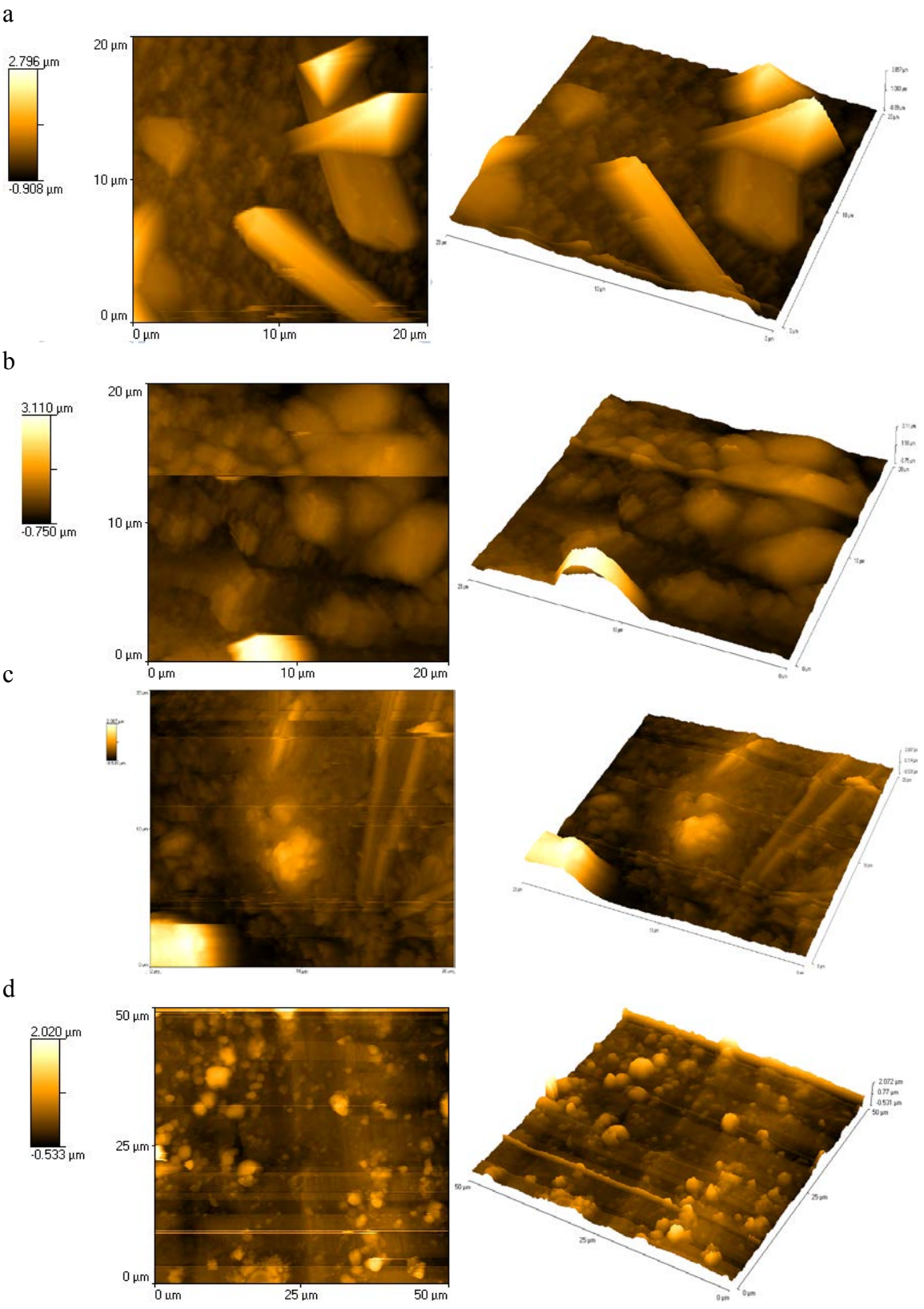

Figure 4.44 AFM analysis of the iridium cluster during the annealing process: (a) nitrogen, (b) helium, (c) hydrogen, (d) argon.

Tables 4.3 and 4.4 summarize the results of stainless steel samples and diamond treated with iridium during the annealing and oxidation process. Note that temperatures and gases were different for each sample during the annealing process, as well as the oxidation time. A change of mass (weight) after the oxidation process reveals the presence of corrosion in the samples.

Table 4.3 Stainless steel treated with iridium

Sample Number	Annealing:(^{0}C/h) temperature/time	Environment	Weight/before oxidation (gr)	Oxidation:(^{0}C/h) temperature/time	Weight/after oxidation (gr)
1 (17Ir)	600/3	Hydrogen	0.08498	815/8	0.08511
2 (22Ir)	800/3	Hydrogen	0.08150	815/4	0.07823
3 (7Ir)	400/3	Argon	0.08272	815/4	0.08310
4 (12Ir)	700/3	Argon	0.07849	815/8	0.07850
5 (9Ir)	600/3	Helium	0.08054	815/4	0.08057
6 (15Ir)	600/3	Helium	0.09342	815/8	0.09368
7 (4N) [a]	500/3	Nitrogen	0.05490	820/8	0.95415
8 (14N) [a]	700/3	Nitrogen	0.06477	815/4	0.06449

[a]: The samples lost mass

Table 4.4 Diamond treated with iridium

Sample Number	Annealing:(^{0}C/h) temperature/time	Environment	Weight/before oxidation (gr)	Oxidation:(^{0}C/h) temperature/time	Weight/after oxidation (gr)
1 (20Ir)	900/3	Hydrogen	0.00926	815/4	0.00643
2 (29Ir)[a]	600/3	Argon	0.00472	815/4	0.00259
3 (36Ir)[a]	500/3	Argon	0.01225	815/8	0.00504
4 (26Ir)[a]	600/3	Helium	0.00663	815/4	0.00280
5 (34Ir)[a]	500/3	Helium	0.00957	815/8	0.00764

[a]: The samples lost mass

CHAPTER 5

Conclusions

Research has shown that one of the main problems in the production of hydrogen from the sulfuric acid decomposition at high temperatures is finding support materials that withstand the high corrosive environmental conditions in the decomposition of an acid at high temperatures. This research showed that diamond and stainless steel materials treated with platinum and iridium, improved their oxidation resistance.

This research has shown that diamond treated with platinum can be used as a support material in the catalysis processes. Also, it can be a suitable material to use as a protecting coat in the sulfuric acid decomposition process.

Diamond treated with platinum improved the corrosion resistance when exposed at the sulfuric acid decomposition in the OXR, for a period of time between four and sixteen hours (Table 4.1). After this process corrosion was not observed. The results of this research proved the key to improve the oxidation resistance of diamond treated with platinum, is an annealing process in a hydrogen atmosphere at 600-700^{0}C for 4 hours. The annealing process created a homogeneous coating of the samples coating of the samples.

EDS results showed that the concentration of platinum changed in the different processes (annealing and oxidation processes), as a result of the impurities and the

formation of platinum clusters or the transformation of the clusters. The formation of platinum clusters is one of the reasons why the surface of the samples changed from smooth to rough, leaving the diamond samples unprotected, and allowing the corrosion process due to the presence of oxygen free radicals. SEM and AFM analyses showed that the samples surfaces changed from homogeneous and smooth to inhomogeneous and rough.

The stainless steel with platinum treatment can be used as a support material in the production of hydrogen from the sulfuric acid decomposition. After the annealing process, the samples did not show signs of corrosion, when they were tested in the OXR for a period of time between 4-12 hours. The SEM and EDS results confirmed that the annealing process created a uniform coating at the samples. Furthermore, these results proved the formation of irregular shape clusters pits and crevices (Figure 4.31), when the stainless steel samples treated platinum were tested in the OXR, without the annealing process. As a result, it was possible to identify corrosion in the stainless steel sample. AFM results showed that the samples surface changed, after the sample was tested in the OXR.

In the cases where the annealing process was in helium or argon atmospheres, the stainless steel treated with platinum showed low corrosion, only in the cases where the annealing temperature was lower than 600^0C.

This research showed that diamond and stainless steel treated with platinum can be used as support materials during the thermochemical sulfuric acid decomposition processes.

The stainless steel treated with iridium, did not show signs of corrosion, when they were tested in the OXR. This absent of corrosion could be the result of the annealing process at high temperature in the hydrogen, argon or helium atmospheres. When the annealing process was in the nitrogen atmosphere, the samples showed low corrosion (Table 4.3). The SEM and AFM showed that in this case, the formation of iridium clusters increased as result of impurities in the nitrogen gas. In the cases where the gas used in the annealing process was different than nitrogen, the samples did not show corrosion after 4-12 hours in the OXR. EDS analysis revealed that the cluster were iridium (Figure 4.42).

AFM showed that the shapes of the clusters are dependant of the gas used in the annealing process, and the temperature.

The MOD:FEDOA process improved the annealing technique at high temperature and high vacuum. SEM analysis in combination with AFM confirmed that the MOD:FEDOA improved the samples coating.

CHAPTER 6

Suggestions for future work

This research discovered a novel method to improve the oxidation resistance of diamond and stainless steel has been development and tested. As result of this discovery, diamond and stainless steel treated with iridium and platinum can be used as support materials in the sulfuric acid decomposition at high temperatures. In addition, this study found that the formation of iridium clusters is higher in the case where the annealing process is a nitrogen atmosphere, in the case of the stainless steel treated with iridium.

Furthermore, this research found a high concentration of iridium clusters formed in stainless steel when treated with iridium. Due to this finding, suggestions for future work include understanding the effect of argon, helium, hydrogen, and nitrogen, in the annealing process at high temperatures of stainless steel when treated with platinum and iridium. The study of the effect of these gases can better explain the formation of clusters in the annealing process. Also, future research should be focus in how the cluster shapes will affect the oxidation resistance of stainless steel.

The next step in this research should be focus in determining the efficiency of the stainless steel treated with iridium or platinum in catalysis process, when it is used in the sulfuric acid decomposition. For this, it is suggested that all samples prepared in this study should be exposed in the oxidation reactor for longer periods of time.

APPENDIX

Appendix I. ENERGY CONSUMPTION

In the last decades energy consumption has increased and will continue to grow by 49 percent from 2007 to 2035 (Figure A.1)[48], and the world energy consumption of fuel will continue to increased (Figure A.2)[48]. As a result, fossil fuel imports have grown and will continue to grow due to the development of emerging economies, especially in Asia.

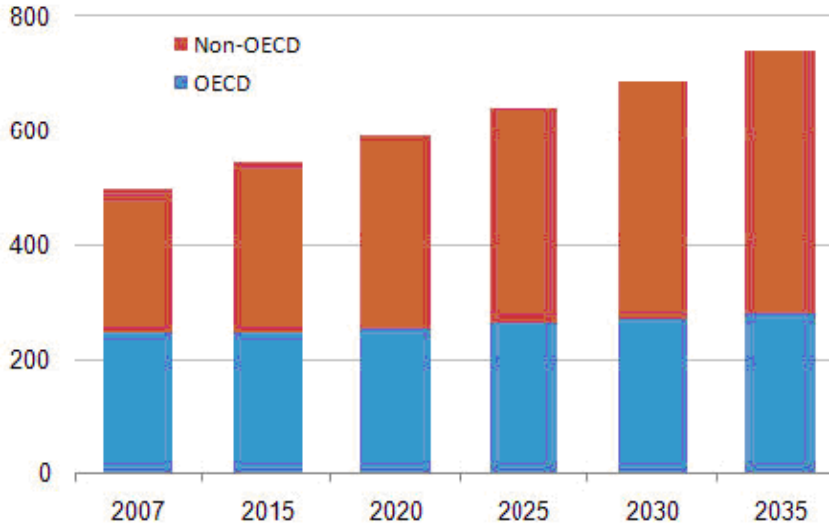

Figure A.1[48]. World marketed energy consumption

In Asia, the consumption of energy sources, especially coal, is growing faster than any other part of the world[48]. The world coal consumption is expected to increase from 132 quadrillion Btu in 2007 to 206 quadrillion Btu in 2035, for an average rate of 1.6% per year[48,49].

Much of the increase expected from 2007 to 2035 and will occur in nations outside the organization for economic cooperation and development (non-OECD nations)[49], which accounts for 95 percent of the total net in the world (Figure A.3)[48]. For example coal used in China's industries has grown by 56.5 percent in the last decade[50].

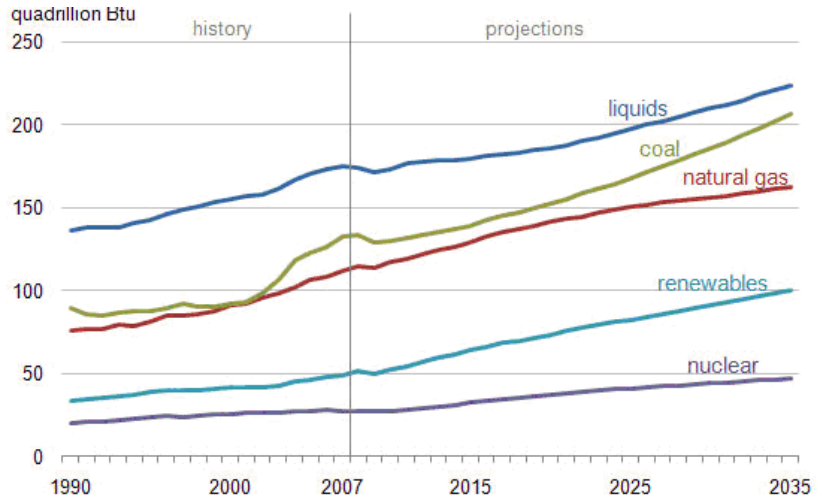

Figure A.2[48]. World marketed energy use by fuel type.

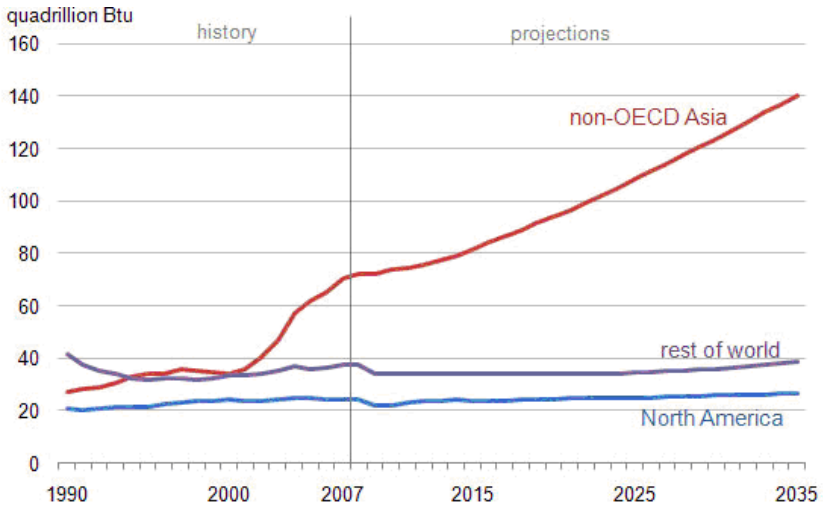

Figure A.3[48]. World coal consumption by region

In recent years, there has been an increase in the production of greenhouse gases (carbon dioxide) in the world (Figure A.4)[48] as a result of the increased consumption of fuels particularly of coal in Asia[50].

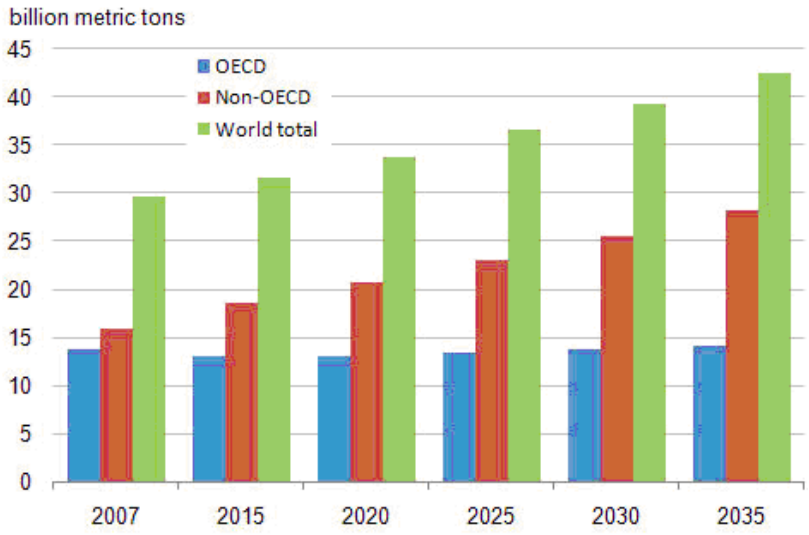

Figure A.4[48]. World energy-related carbon dioxide emissions.

Carbon dioxide (CO_2) is one of the gases that contribute most to the greenhouse effect[2]. The CO_2 levels have been rising from 29.7 billion metric tons in 2007 to 33.8 billions metric tons in 2020[1, 2] (Figure A.4)[1]. For this reason, there is a need to find a new source of energy to reduce the production of greenhouse gases, with a significant reduction of global use of fossil fuels.

APPENDIX ll. PROPERTIES OF MATERIALS

In the last five years, the MU-DRG has been used to study materials that can withstand the conditions of the sulfuric acid decomposition cycle for hydrogen production. The surface modification of some materials increases the resistance to corrosion, when they are exposed to harsh environments, such as the case in the nuclear reactor used to produce hydrogen from sulfuric acid.

Platinum and iridium are some of the materials that the MU-DRG use to improve the resistance of diamond, stainless steel and quartz when these materials are used for the sulfuric acid decomposition cycle..

Platinum is an extremely rare metal found in a concentration of 0.005[32] in the earth's crust. It is one of the densest and heaviest metals, highly malleable and ductile. Platinum has a high resistance to corrosion even at high temperatures (table B.1). This property makes the platinum can be used as a catalytic for industrial applications. For example, the production of hydrogen from sulfuric acid cycle. Platinum is corroded by halogens, cyanides and caustic alkalis. Platinum is insoluble in nitric and hydrochloric acid, but dissolve in aqua regia [33]. Platinum is used in electric contacts, electrodes, catalytic converters, as a catalyst in petroleum refining, and in fuel cells.

Table B.1. Properties of platinum[35] and iridium.

Properties	Platinum	Iridium
Atomic number	78	77
Atomic mass	195.08 amu	192.217
Melting point	1772 C	2466C
Boiling point	3827.0C	4428C
Density	21.45 gr/cm3	22.56 gr/cm3
Electrical resistivity	9.85 microhm.cm at 0C	47.1nΩ·m at 20C
Thermal conductivity	73 watts/meter/C	147 $W \cdot m^{-1} \cdot K^{-1}$
Thermal expansion	8.8μm./mk at 25C	6.4 μm/(m·K)
Color	Silver white	White

Iridium is one of the least abundant elements in the earth's crust, having an average mass fraction of 0.001 ppm in the earth's crush[36]. Iridium is the most corrosion-resistance metal known, even at high temperatures (table B.1). Iridium would be attacked by some molten salts such as potassium cyanide and sodium cyanide[36]. Iridium has been used for different application such as: electrical (spark plugs), electrochemical (electrodes for the chloralkali process), for catalysis and Iridium is used in particles physics for the production of antiprotons a form of antimatter.

Stainless steel does not corrode, stain or rust easily as the ordinary steel. It is called corrosion-resistant steel (CRES). The high oxidation resistance in air at ambient/room temperatures is achieved with the addition of a minimum of 13 %(by weight) chromium, and 26% if is used for harsh environments 39 (Stainless steel applications ranging from kitchen to surgical instruments.). There are several types of stainless steel, but the most resistant to corrosion are the 304 and 430. Their composition and properties are similar to each other (Table B.2) [37]

Table B.2[37]. Steels steel composition

Grade	C (%)	Mn(%)	Si (%)	P(%)	S(%)	Cr(%)	Ni(%)
304	0-0.08	0-2.0	0-0.75	0-0.045	0	18-20	8.0-10.5
430	0.048-0.12	0.42-1	0.36-1	0.024-0.040	.010-0.030	16-18	-17-0.75

References

1. Hydrogen Economic Fact Sheet "U.S-EU Summit Cooperation on the development of a hydrogen Economy" (http://georgewbush-whitehouse.archives.gov/news/releases/2003/06/20030625-6.html), last visited June 2011
2. K.R. Schultz, L.C. Brown, G.E. Besenbruch and C.J. Hamilton. "Large-scale production of hydrogen by Nuclear energy for the hydrogen Economy". General atomics project 49009 February 2003
3. M. Peck. "Materials study supporting thermochemical hydrogen cycle sulfuric acid decomposition design." Unpublished dissertation, December 2007
4. CAN "Climate technology sheet #9: Hydrogen production" CAN-Europe Tech Sheet 09-version 11-29 2003.
5. L. M. Crosbie. "Hydrogen production by nuclear heat." MPR, January 6, 2003
6. US Department of Energy, Energy Efficiency and Renewable Energy (http://www1.eere.energy.gov/hydrogenandfuelcells/production/natural_gas.html)
7. US Department of Energy, Nuclear hydrogen R&D plant march 2004 (www.hydrogen.energy.gov/pdfs/nuclear_energy_h2_pland) last visited January 2012
8. Y. M Suárez, A. Méndez, M. Prelas, T. Ghosh. "Platinum deposition on Sp3-bond Carbon: Applications in corrosive environments and catalyst support material" American Nuclear Society (ANS), Annual Meeting. November 2007

9. J. Wang and M. Greg. "Swain «Fabrication and Evaluation of Platinum' Diamond Composite Electrodes for Electro catalysis." J. of the Electrochemical Society, 150 E24-E32 ~2003
10. N. Kiyoharu, H. Takayuki, K. Chiaki , I. Na-okhi , K. Testsuhiko, N. Mikka, S. Toshimitsu and A. Toshihiro. "Diamond-Supported metal catalysis: a novel medium for hydrogen production from methanol decomposition." Catalysis letters 80, No. 3-4, June 2002
11. Y. M Suárez, M. Prelas, T. Ghosh. "Platinum deposition on Sp3-bond Carbon: Applications in corrosive environments". Proceedings of the twentieth annual meeting of Nasa-Missouri Space Grant consortium. April 2011
12. Y. Yurum. "Production and utilization of hydrogen and future aspects". Hydrogen energy system. Department of chemistry, Hacettepe University, Ankara, turkey. Kluwer academic publishers, 1995
13. P. M. Mathias and L.C. Brown "Thermodynamics of the sulfur-iodine cycle for thermochemical hydrogen production." 68th Annual Meeting of the Society of Chemical Engineers, Japan. March 2003.
14. X. Vitart, A. Le Duigou, P. Carles. "Hydrogen production using the sulfur-iodine cycle couple to a VHTR: An overview." Energy conversion and management, 47, 2740-2747, 2006
15. L. M. Crosbie and Dr. D. Chapi. "Hydrogen production by nuclear heat." GENE/ANP2003, Kyoto, Japan. September 2003. (http://www.mpr.com/news-and-publications/white-papers/H2-from-Nuclear.pdf)

16. W. A. Summer, M. R. Bucher. “Hybrid sulfur thermochemical process development.” *DOE Hydrogen Program FY 2005 Progress Report* 323. ((http://www.hydrogen.energy.gov/pdfs/progress05/iv_g_7_summers.pdf)
17. Y.H. Jeong, M.S. Kazimi , Hohnholt K.J., and Yildiz, B. “Optimization of the hybrid sulfur cycle for hydrogen generation.” Nuclear energy and sustainability (NES) Program, May 2005
18. N. S. Rashkeev, D. M. Ginosar, L. M. Patrovic, and H. H. Farrel. “Catalytic activity of supported metal particles for sulfuric acid decomposition reaction.” Catalysis today 2008
19. S. Lee, H. Permena and K. Y. Simon. “Effects of annealing and gas treatment on the morphology of platinum cluster size on highly oriented pyrolytic graphite by scanning tunneling microscopy”. Catalysis letters 23, 281-292, 1994.
20. T.P. Chojnacki. and L.T Schimidt. “Microstructure of Pt-Rh particles on $SiO^{1}_{2.}$” Journal of Catalysis, 115, 473-485, 1989
21. T.P. Chojnacki and L.D. Schmidt. “Microstructures of Pt-Sn and Rh-Sn particles on SiO_2”. Journal of Catalysis, 129 (2), June 1991
22. W. Sripumkhai and e.t. “Effect of annealing temperature on platinum thin films prepared by electron beam evaporation.” Journal of the microscopy society of Thailand (1), 51-54, 2010
23. M. Drescher. “Surface nobilities on solid materials” Ed. Vu Thien Binh (plenum press, New York), 1993
24. N. Rashkeev and et. “Catalytic activity of supported metals particles for sulfuric acid decomposition reaction”, Catalysis today 2008

25. D. R. O'keefe, J. H. Norman and D. G. Williamson. “Efficient catalytic decomposition of sulfuric acid with copper.” Catalytic. Rev, 22, 325, 1980

26. B.M. Nagaraja. “Catalytic Decomposition of SO_3 over $Pt/BaSO_4$ materials in Sulfur−Iodine Cycle for Hydrogen Production.” Ind. Eng. Chem. Res. 48, 1451-1457, 2009

27. A.M BARNERJEE, and e.t. al. “Catalytic decomposition of sulfuric acid on mixed Cr/Fe oxide samples and its application in sulfur–iodine cycle for hydrogen production.” International Journal of Hydrogen Energy 33, 319-326, 2008

28. T.M. Lillo. K.M. Delezene-Briggs. “Commercial Alloys for Sulfuric Acid Vaporization in Thermochemical Hydrogen Cycles.” INL Idaho National Laboratory. October 2005

29. A. E. Mendez Torres. “Microengineering of diamond”. Unpublished dissertation. August 2008

30. www.unctad.org/infocomm/anglais/platinum/characteristics.htm (last visited July 2010)

31. N. Greenwood, A. Earnshaw. “Chemistry of the Elements” Oxford: Butterworth-Heinemann. pp. 1113–1143, 1997

32. J. Emsley. "Iridium". Nature's Building Blocks: An A-Z Guide to the Elements. Oxford, England, UK: Oxford University Press. pp. 201–204, 2003.

33. www.platinum.matthey.com/uploaded_files/Pt2008/08_complete_publication.pdf. Retrieved 10-13 2008

34. http://www.azom.com/Details.asp?ArticleID=4243#_404GP_Stainless_Steel (last visited September 2011)

35. M.A Prelas, G. Popovici, and T. Sung. “Forced diffusion of impurities in natural diamond and polycrystalline diamond films”, J. Appl. Physics, 77, 1995
36. L.C. Brown, and et. “Alternative Flow sheets For the Sulfur-Iodine Thermochemical Hydrogen Cycle.” Spring National Meeting of AIChE, New Orleans, Louisiana, March 4 through April 3, 2003
37. Schwartz D, Gadiou R, and et al. “A kinetic study of the decomposition of spent sulfuric acids at high temperature.” American Chemistry Society, 39 (200) 2183-2189
38. Chunlei W, and Toshimichi I.“Chemical-deposited diamond overgrowth on platinum thin films deposited on diamonds substrates.” Japanese Journal of Applied Physics, 39(2000) 1286-1290
39. Follador R.C, and et. al. “Preliminary study of CVD diamond film to improve the performance of heat flux sensors for hypersonic experiments.” Diamond & Related Materials 14, 637–640, 2005
40. A. Mendez, M. Prelas, T. Ghosh, L. Ross. “A method for finding N-type and P-type impurities for wide band-gap materials, such as diamond.” MRS spring meeting, San Francisco, Ca, May 2005
41. J.E. Maslar, W.S. Hurst, W.J. Bowers and J.H. Hendricks. “In situ raman spectroscopic investigation of stainless steel hydrothermal corrosion”. Corrosion Science section, Vol. 58, No 9 2002
42. C. Wang and T. Ito. “Chemical-vapor-deposited diamond overgrowth on platinum thin films deposited on diamond substrates”

43. T. Dhanabal, G. Amirthaganesan and J. Ravichandran. “Pitting corrosion protection of low nickel stainless steel by electropolymarized conducting polymer coating in 0.5 M NaCl solution.” Bull. Mater. Sci, Vol 34, No. 3, June 2011

44. Y. M Suárez, M. Prelas, T. Ghosh. “Platinum deposition on Sp3-bond Carbon: Applications in corrosive environments”. Proceedings of the twentieth annual meeting of Nasa-Missouri Space Grant consortium. April 2011

45. R.M. Tiggelaara, and et… “Stability of thin platinum films implemented in high-temperature microdevices”. Sensors and actuators A 152, 39-47, 2009

46. S. Music, S. and et… “Thermochemical formation of IrO2 and Ir”. Materials letters 57, 5409-4514, February 2003

47. T. Tai-Jui wang and et… “Formation of iridium nanocrystals with highly thermal stability for the applications of nonvolatile memory devices with excellent trapping ability”. Applied Physics letters 97, 143507, 2010

48. U.S Energy information administration/2010 (http://www.eia.gov/oiaf/ieo/highlights.html), last visited may 2010

49. U.S. Environmental protection agency, basic information on climate change (http://www.epa.gov/climatechange/basicinfo.html)

50. S. Giljum, M. Dittrich, S. Bringezue, C. Polzin and S. Lutter. “Resource use and resource productivity in Asia”. SERI Working Paper Series “Working paper number 11” May 2010

VITA

Yefer Mauricio Suarez Buitrago was born on June 29, 1971, in Tunja,Colombia. He was attending at the INEM “Carlos Arturo Torres” Tunja high school. After his high school, He earned his bachelor in Physics and Mathematics from the Universidad pedagogica y tecnologica de Colombia-Tunja, Master in Physics from the University of Puerto Rico- Mayaguez. In Missouri, he earned a PhD. In Nuclear Engineering from University of Missouri-Columbia.